(NASA-CR-148196) ANALYTICAL WORK IN SUPPORT OF THE DESIGN AND OPERATION OF TWO DIMENSIONAL SELF STREAMLINING TEST SECTIONS Semiannual Progress Report, Oct. 1975 - Mar. 1976 (Southampton Univ.) 67 p HC $4.50 G3/09

N76-26223

Unclas
44140

UNIVERSITY OF SOUTHAMPTON

department of aeronautics and astronautics

ANALYTICAL WORK IN SUPPORT OF
THE DESIGN AND OPERATION OF
TWO DIMENSIONAL SELF STREAMLINING
TEST SECTIONS

NSG - 7172

Semi-annual Progress Report

October 1975-March 1976

ANALYTICAL WORK IN SUPPORT OF THE DESIGN AND OPERATION OF TWO DIMENSIONAL SELF STREAMLINING TEST SECTIONS

by

M. Judd
S.W.D. Wolf
M.J. Goodyer

Department of Aeronautics and Astronautics
The University
Southampton, U.K.

This is a Semi-annual Progress Report, October 1975-March 1976, on work undertaken on NASA Grant NSG-7172 entitled "The Self Streamlining of the Test Section of a Transonic Wind Tunnel". The Principal Investigator is Dr. M.J. Goodyer.

CONTENTS

1. Introduction

2. A Method for Computing the Imaginary Flowfields

3. Interference Effects of Wall Position Errors

4. Estimations of Interference Introduced by the Truncation and the Choice of Test Section End Geometry, Including Compressibility Effects.

5. A Predictive Method for Rapid Wall Adjustment

6. Conclusions

List of Symbols

List of References

Figures

1. INTRODUCTION

This report covers analytical work which has been undertaken in connection with the flexible walled self streamlining two dimensional test section. The report period is the first half-year of what may become a two or three year project, and hence the bulk of the work carried out, and the emphasis of this report, is of a theoretical nature. Separate chapters of the report relate to aspects of the operation of flexible walled test sections and to the design of a proposed transonic test section.

The aim of the self streamlining wind tunnel is to reproduce within the limited extent of the test section the flowfield that would have existed around the same model in an infinite flowfield. The methods, as discussed here, are applied to two-dimensional testing. The principal difference between the self streamlining wind tunnel and conventional tunnels for two dimensional testing is that the former has flexible top and bottom walls. The flexible walls are impervious, and are positioned by jacks to the contours of appropriate streamlines which would have existed around the same model in an infinite flowfield. A method for selecting wall contours - a criterion indicating that they are streamlines - is required because of the infinite number of possible contours.

The infinite two dimensional flowfield may be imagined to be divided into three portions: two 'imaginary' portions extending from the test section upper and lower walls out to infinity, separated by a real portion of flowfield which is that

in the test section. The selected streamlining criterion[1] is an adjustment of the wall contours until the measured pressures along the upper and lower boundaries of the test section, that is along the flexible walls, match pressures along the adjacent and identically shaped boundaries of the imaginary flowfields. The imaginary fields have the same free-stream conditions as the real flowfield.

In a wind tunnel test an attempt is made to reproduce the real portion as accurately as possible. It then remains to check on the correctness of the wall contours by comparing real and imaginary wall pressure distributions. There are several ways in which the pressure distributions in the imaginary fields may be derived. For example, they may be determined empirically by reproducing each of the two fields in water or in air. The latter approach, which can in principle yield information applicable to low speed or to high speed flows, has been tried[1]. Alternatively, for low speed testing the electrolytic tank can be employed since the flowfield to be reproduced is essentially free from viscous effects. However, the alternate approach of computing the imaginary flowfields has been adopted. Arguments supporting this choice include the fact that inviscid flows can be computed with some certainty, and also the ease with which the computational step may be included in any closed-loop control of the flexible walls.

The imaginary flowfields are computed flowing over the effective contours of the walls. The effective contour is composed of the physical shape of the wall modified by the displacement thickness of its boundary layer. The present

method[1] requires only an estimation of the differences in displacement thickness between runs with the test section empty and with the model present. The differences are applied as corrections to the geometrical contours to give effective contours. The corrections are applied only to the flexible top and bottom walls. In the present tunnel[1] the sidewall area is one-third of the total area and the effects of possible changes in the state of the sidewall boundary layers have so far been ignored.

The application of the above procedures leads the walls via a series of iterations to streamline shapes, but with possible residual imperfections arising from:

i) Resolution of wall pressure measurements

ii) Resolution of wall position measurements affecting
    a) the imaginary flowfield computations
    b) the flow at the model

iii) Errors in estimations of changes of boundary layer displacement thickness on the flexible walls, or changes in the sidewall boundary layers, affecting
    a) the imaginary flowfield computations
    b) the flow at the model

iv) Effects of the truncation of test section length and of the constraints imposed by the portions of wind tunnel upstream and downstream of the test section.

v) Only a finite number of wall co-ordinates are defined.

This report is concerned with theoretical work undertaken in support of the development of this method of interference-free testing. In Chapter 2 of the Report is described the method

currently in use for computing the imaginary flowfields from the effective wall contours, while in Chapters 3 and 4 are analytical assessments of the effects of two of the possible sources of imperfection in streamlining listed above, namely (ii) (b) and (iv) respectively. Finally, in Chapter 5 there is described a proposed method for accelerating the wall iteration procedure which, if successful, will replace the existing method.

2. A METHOD FOR COMPUTING THE IMAGINARY FLOWFIELDS

2.1 Non-Lifting Models

The division of the infinite two-dimensional flowfield into upper and lower imaginary parts, I_u and I_ℓ, separated by real part R is illustrated on Figure 2.1. The requirement is to compute I_u and I_ℓ to yield the pressure distributions given by the imaginary fields at their wall boundaries. As noted in the Introduction the input data to the computation of a field includes the free stream conditions and also the effective contour of the adjacent wind tunnel wall.

The particular computational technique which has been adopted regards the tunnel wall as a boundary to an otherwise infinite two-dimensional field. Testing to date has been confined to low speeds, and it has already been noted that the flow in this region of an infinite flowfield surrounding the model under test would behave essentially as though inviscid. Therefore the computations are based on two-dimensional incompressible potential flow theory. The wall is represented in the theoretical model by the envelope of the flow from a set of sources and sinks distributed along a straight line lying parallel to the freestream and positioned fairly close to the wall. This model is illustrated in Figure 2.2, which shows the wall contour, and the upper half of the source envelope. The wall co-ordinates are known at a finite number of points, and the strengths of the source/sink set can be adjusted until co-ordinates of the envelope of the source/sink flow coincide with the wall co-ordinates. It is then an easy step to compute the

pressure distribution along the contour for comparison with that measured inside the test section. The program is identified as SS1.

This notional approach has been tested in the following manner. The shapes of streamlines representative of the desired locations of the flexible test section walls, and also the pressure distributions along the walls, have been computed exactly for inviscid flowfields around several different bodies. The streamline shapes were then taken as input data to a program based on the above source/sink model to compute the wall pressures. One of the bodies is shown on Figure 2.3. It comprises a source at the origin mid-way between test section walls, followed by a sink having half of the strength of the source. The sink is distance $^{h}/_{2}$ downstream of the source, where h is the nominal depth of the test section. The body is not lifting. The contour of part of the upper wall is shown. On Figure 2.4 more of the contour is shown, in the form of a measure of the deflection Δy of the streamline by the model. Far upstream the streamline asymtotes to a height $^{h}/_{2}$ above the axis. Note the magnified deflection scale which has its origin at height $^{y}/_{h} = 0.5$.

A set of 15 sources or sinks were positioned along the $^{x}/_{h}$ axis of Figure 2.4 at the indicated locations. The program was arranged to adjust the strengths until the envelope passed through 15 specified wall positions, within some tolerance. Computed values of wall streamline pressure coefficients are shown on the lower part of Figure 2.4. The continuous line is an exact solution for potential flow about the body. Sets

of pressure coefficients computed from SS1 are also shown for two matching tolerances between source envelope and wall contour. These are $\pm c/1{,}800$ and $\pm c/18{,}000$, where c is the wing chord for which the test section was designed, 137.16mm (5.4 inches), giving tolerance:chord ratios of $\pm 5.6 \times 10^{-4}$ and $\pm 5.6 \times 10^{-5}$. It can be seen that with the use of a tight tolerance in SS1 the pressure predictions are almost exact, whereas with the contour matched by an envelope to within the lower level of accuracy ($c/1{,}800$), which happens to correspond approximately to the accuracy experienced[1,2] in the setting of walls in some low speed testing, noticeable errors occur in the computations. The average of the modulus of the error in the computed pressure coefficients at fifteen locations along the wall was 0.0035 and 0.0004 with the $\pm c/1{,}800$ and $\pm c/18{,}000$ tolerances respectively. Until the implications of such errors are properly understood, it is proposed to retain a fairly tight tolerance in the computing, despite a lengthening of the computation time with reduction of tolerance.

2.2 Lifting Models

When applied to the analysis of wall pressures for lifting models, SS1 yielded results which were unsatisfactory in terms of pressure errors. Increasing the number of source/sinks along the wall introduced only a small improvement. On Figure 2.5 is shown one of the mathematical models used in this part of the analysis, a lifting cylinder. The wall contours were matched by the source/sink envelope this time to within a tolerance of $\pm c/2{,}700$. Note with lifting bodies the upper and lower wall contours and therefore the two imaginary flowfields differ.

Examples of the computations are shown on Figure 2.6 for the lower wall. A representative length of test section wall is shown with a magnified y-scale, together with the positions of 29 sources/sinks distributed along a horizontal tangent to the crest of the contour. The length of contour is about 7h. The exact pressure distribution is shown on the lower half of Figure 2.6 together with that given by SS1 modified for the use of 29 sources and sinks. It can be seen that the values of C_{pi} predicted by SS1 in this form are considerably in error, the errors averaging about 0.02 and therefore lying well outside the limits of experimental pressure resolution.

For the case of lifting bodies it was found necessary to represent in the analysis a length of wall much longer than the test section to bring the computed values of imaginary flowfield pressure coefficients inside the experimental limits of resolution. The latter is about ± 0.01[1].

Satisfactory predictions were obtained with the addition of more sources/sinks, 14 upstream and 14 downstream evenly spaced, allowing the envelope to match the streamline at a total of 57 points over a total length of 33h. An example of a computation is shown on Figure 2.6, where the average C_p error is about 0.004 in the region of the test section, and the maximum local error is less than 0.01.

While the preceeding types of computation had served to indicate the requirements in terms of the length of streamline matched by the source/sink envelope in the case of lifting models, it was not possible to immediately implement the method since in practice the wall contour is obtained from measurements on

the test section, and therefore only a portion of the contour required by this version of SSl is known. The shapes of the streamline contours beyond the ends of the test section are estimated in the following manner. The circulation Γ around the test section boundary is calculated from measurements in the test section, giving the lift on the model. The circulation is assumed centered in a vortex positioned in the model. The shapes of the streamlines extending upstream and downstream from the ends of the test section walls are assumed to be dominated by the combination of the freestream and the vortex. As a further approximation the slopes of the streamlines at distance x downstream from the vortex are taken to be $\Gamma/2\pi xU$, where U is the free stream velocity and the circulation is anti-clockwise positive. It can be shown[3] that for low values of streamline slope, the strength m(x) of an elemental source at x is given by $m(x) = -\Gamma/\pi x$. The disturbance velocity u in the freestream direction, produced at station x along the test section by this source distribution extending to infinity from the end of the test section station x = a is

$$u(x) = \frac{\Gamma}{2\pi^2} \int_a^\infty \frac{d\xi}{\xi(\xi - x)}$$

$$= \frac{\Gamma}{2\pi^2 x} \ell n \left[\frac{a}{a - x}\right] .$$

This method of approximating the effects of the streamlines upstream and downstream of the test section, coupled with the finite source/sink set along the test section, has proved satisfactory in a sufficiently wide range of test cases. These included computations of upper and lower imaginary flowfield wall pressures, for streamlines around models having various amounts of blockage, lift, and wake thickness. The computer program as now developed yielded in all cases an average error in pressure coefficient along the test section of less than 0.01, which is regarded as satisfactory.

The method of wall adjustment has been to move the wall locally a distance proportional to the local difference between the real and imaginary pressures at the wall. The movement of the wall is towards the higher of the two pressures. This method resulted in convergences of the walls to streamlines, but in a relatively large number of iterative steps. Chapter 5 details a method which should increase the rate of convergence.

3. INTERFERENCE EFFECTS OF WALL POSITION ERRORS

3.1 The Nature of the Problem

It is recognised that the flexible-walls can only be positioned by the jacks within some set tolerance, and in this chapter is outlined a method by which the interference introduced by such errors may be estimated. In any given test section of this type there are likely to be many jacks along each wall. In the existing low speed test section there are 15. Position errors are likely to arise in a random manner, both in location and magnitude, within the tolerance band.

While the designer is to a large extent free to choose this tolerance, he must bear in mind that complexity and therefore cost will increase as the tolerance is reduced. Further, since the flexible wall is positioned at a finite number of jacking points there is no control over the shapes of the portions of wall between jacks, which would probably render pointless any endeavour towards levels of precision above some value.

In the existing low speed test section the wall setting accuracy is estimated to be approximately ±0.127mm (±.005 inches) giving a dimensionless tolerance:chord ratio of $\pm 9.3 \times 10^{-4}$, and the same tolerance has been adopted in the following analysis.

In this analysis the wall setting errors are regarded as producing a bump or series of bumps in an otherwise flat walled two-dimensional test section. Even though the bump height would in practice be random, here only the worst case of a maximum error, which is equal to the tolerance, is considered.

In practice a single jack in error along a nominally flat wall might produce a local wall shape similar to a portion of a sinusoid, with the peak or trough of the wave located at the jack. In this analysis such a wall contour disturbance is represented by an equal strength source/sink pair lying on the wall line, with a minimum pair spacing equal to the jack spacing. The strengths of the source and sink were chosen to give an arbitrary bump height equal to 0.00093C. It is recognised that this analytical representation of the effect of a jack error is less than ideal, but it is believed the representation gives reasonable results.

The effects of the presence of the bumps are assessed in the form of three measures of interference in the empty test section at what would be the location of the wing model, assumed central in the test section. The measures of interference are:

a) Angle of attack error at the wing leading edge.

b) Induced camber, which is assumed to be the difference between the flow angles at the leading and trailing edges.

c) Disturbance to free stream velocity, assessed as a dynamic pressure error at the wing quarter-chord point.

Even though the interference effects are quoted for this single but representative value of bump height, since the bumps are small the interference effects are expected to vary linearly with height, allowing simple scaling for other values of wall setting errors.

The interference at the model will depend on the number of jacks in error, on their location, and on the sign of the

setting error. With many jacks per wall, any of which can be in error, it is clear that a very large number of different values of interference is possible.

The approach used here is to analyse a simple bump configuration which intuitively gives an interference close to the maximum. The probability of occurrence is then considered.

3.2 Analysis of Simple Bump Configuration

To find values for the worst effects at the model, investigations were made into the nature of each interference, using an inviscid flow model to determine velocity components and distributions.

The flow model for the simple case of a single bump in one flexible wall consists of a source/sink pair combined with a system of images, thereby producing a test section as shown in Figure 3.1. The parameters available in the analysis are test section height h, the approximate bump length d (measured between source and sink) and the bump position x_b (determined by the source location). It would appear logical to non-dimensionalise with respect to tunnel height, but the severity of the interference is a function of model size and therefore wing chord c was used instead.

Typical magnitudes of each interference and their variations with bump location are shown in Figs.3.2a, b and c, for particular values of $^{h}/_{c}$ and $^{d}/_{c}$. The graphs clearly show that a maximum effect occurs for each interference, as the bump passes underneath the wing model.

The approximate bump positions for the maxima are illustrated in Fig.3.3 for values of $^{h}/_{c}$ in the region of 1. The maximum angle of attack error occurs when the leading edge of the wing is over the nose or tail of the bump. The induced camber is a maximum when the wing leading edge is approximately over the nose of the bump or the trailing edge is over the tail. The maximum velocity increment occurs when the quarter chord point is over the bump mid-point. The forms of Figs.3.2a, b and c also suggest that the interferences are significant in most cases for a total range in $^{x_b}/_{c}$ of about 1.

It is therefore assumed that jack errors outside of a tunnel length of about 2 chords will not produce any significant interference, and it does not matter whether these jacks are in error or not, within the assumed tolerance.

The variations of the three maximum interferences with bump length and model size are shown in Fig.3.4a, b and c. It can be seen that the interferences reach near-maximum values at $^{d}/_{c}$ in the region of unity.

It is now possible to consider the probabilities for the occurrence of combinations of jack errors leading to significant interference. It is assumed that each jack error is statistically independent and, in order to obtain a conservative estimate, that the magnitude of each error is equal to the tolerance. In practice, there would be a distribution of errors ranging in magnitude from zero up to the tolerance. Over a tunnel length of two chords near the model, let there be N jacks. The probability of a particular jack being in error (up or down) is 1/N. The probability of

all the other jacks being in error in the opposite sense is $1/2^{N-1}$. However, it has already been seen that any single bump will produce a significant interference over a range of about 1 chord and could therefore be produced by any one of N/2 jacks. The probability of a significant interference occurring because of a single jack bump is therefore

$$P_1 = \frac{1}{N} \cdot \frac{1}{2^{N-1}} \frac{N}{2} = \frac{1}{2^N}$$

The probability of a second jack adjacent to the first having an error of the same sign is $1/(N - 1)$. The probability of a two jack simple bump is therefore

$$P_2 = \frac{1}{N} \frac{1}{(N - 1)} \cdot \frac{1}{2^{N-2}} \frac{N}{2} = \frac{1}{2^{N-1}(N - 1)}$$

The probability of an n jack simple bump is

$$P_n = \frac{(N - n)!}{2^{N-n+1}(N - 1)!}$$

and the relative probability is

$$\frac{P_n}{P_1} = \frac{2^{n-1}(N - n)!}{(N - 1)!}$$

These results are given for various N in Table 1 in the form of the inverse of the probability, i.e. in terms of the likely number of wall adjustments to produce a maximum error.

Table 1

	N = 6	N = 12
$1/P_1$	64	4096
$1/P_2$	160	22528
$1/P_3$	320	112640

3.3 A Summary of Interference Effects

Current aims are to use minimum test section depths roughly equal to a wing chord and jack spacings of around ¼ chord. The arguments of the previous section and the results in Table 1 suggest that for jack spacings of 3 or 4 per chord, the probability of a multi-jack simple bump is sufficiently high that the maximum error values in Figs.3.4a, b and c should be taken. Therefore it is felt that the interference effects given by such a bump in one wall of a test section with depth of one chord should be adopted in test section design. The interference effects are then

angle of attack error	0.025 degrees
induced camber	0.05 degrees
C_p error	0.0018

These three effects can be related by converting them into equivalent errors in C_L. The conversions have assumed a lift curve slope of 2π for the angle of attack error, thin airfoil theory (similar to that in Section 4.2.1) in converting induced camber, and a uniform C_p error in forming an equivalent C_L error. Note that the latter approximation will lead to a high estimate for the C_L error. The resultant figures are

C_L error due to angle of attack error	0.00275
C_L error due to induced camber	0.00125
C_L error due to C_p error	0.0018

These levels of interference may be considered acceptably small, and therefore it is felt that despite the fact of the analytical model not giving a shape of bump very close to that which might be expected in practice, it is unlikely that a more realistically shaped bump could give a less acceptable level of interference.

If on the other hand the interferences are not acceptable, because it is impossible to apply corrections the tunnel must be designed to reduce the errors. The preceeding reasoning indicates that this may be achieved at lowest cost by installing position monitors of enhanced accuracy only at those jack locations close to the model.

4. INTERFERENCE DUE TO WORKING SECTION END CONDITIONS

4.1 Introduction

The theoretical bases for the adjustment of the wall contours to produce streamline surfaces are now well established and the remaining problems lie in their practical implementation and in improving the efficiency of associated computational procedures. The tunnel will comprise a working section with self-streamlining walls in the vicinity of the model with tailoring at each end to meet the fixed portions of the tunnel circuit. In the modification of an existing tunnel or design of a new one, careful consideration must be given to these end conditions and various configurations are possible. The features to be investigated in this chapter are:-

1) The best type of end structure, e.g. solid wall, open jet or a combination.

2) The minimum length of adjustable section to produce an acceptably low level of tunnel interference from the non-streamline contours.

3) The effect of compressibility on the length requirements.

These features will be considered in turn from the viewpoint of model interference corrections only and not from that of detailed mechanical or constructional advantages. However, the favoured configuration from the aerodynamic standpoint is also relatively easy to implement in practice.

4.2 Possible Terminal Structures for the Streamline Section

Possible configurations are represented diagrammatically in Fig.4.1. They comprise (a) solid/open jet ends, (b) solid/solid ends and (c) solid/open jet ends with flow turning. In the case of (a) and (b) short transition sections between the fixed ends and the adjustable walls would be necessary, but in (c) the turning angle could be adjusted so that the wall slopes are tangents to the streamlines at entry to and exit from the adjustable section. These configurations are by no means exhaustive; porous sections will not be considered. However, they are representative of extreme cases and the solid terminators are amenable to analysis.

4.2.1 Basic case for analytical solution

Approximate and, in some cases, exact estimates of the tunnel interference can be obtained from the basic two-dimensional arrangement shown in Fig.4.2, where distributed velocity is shown imposing constraints of streamwise flow at the test section entry. It is probable that solid and wake blockage can be readily minimised and therefore the lift interference is a more critical case. The nature of this interference is indicated in Fig.4.2, for the solid inlet/free streamline configuration. The net effect of the wall vorticity is to produce (for the sense of model circulation shown)

(i) an upwash at the model

(ii) an effective negative camber at the model due to the upwash gradient.

Both make contributions to the interference and their magnitudes are assessed using the following analysis.

A complex z-plane representation of the two-dimensional tunnel section is shown in Fig.4.3(a) with the origin of the axes at E. The centre of the model lift is at G, given by $z = z_o$ where $z_o = a + \frac{ih}{2}$. The z-plane is transformed into the upper half of the ζ-plane by:-

$$z = \frac{h}{\pi}\left[\frac{(1 - \zeta^2)}{2} + \ln\zeta\right] \qquad 4.1$$

The point G transforms to $\zeta = i\eta$ where η is given by:-

$$a = \frac{h}{\pi}\left[\frac{(1 + \eta^2)}{2} + \ln\eta\right] \qquad 4.2$$

The flow resulting from an isolated vortex of strength Γ at z_o with solid boundaries at ABC and DEF can be obtained from a vortex of strength Γ at $i\eta$ in the ζ-plane with its mirror image of strength $-\Gamma$ at $-i\eta$. The complex potential is:-

$$w = \phi + i\psi = -\frac{i\Gamma}{2\pi}\{\ln(\zeta - i\eta) - \ln(\zeta + i\eta)\} \qquad 4.3$$

The total velocity components in the z-plane are given by:-

$$u - iv = \frac{dw}{dz} = \frac{dw}{d\zeta} \cdot \frac{d\zeta}{dz}$$

The wall interference is obtained from the velocity components at G in the z-plane after subtracting the velocity field of the model vortex. The resultant components are formally:-

$$\bar{u} - i\bar{v} = \lim_{z \to z_o} \left[\frac{dw}{d\zeta} \cdot \frac{d\zeta}{dz} + \frac{i\Gamma}{2\pi} \frac{1}{(z - z_o)} \right] \qquad 4.4$$

The upwash component is $\bar{v}$. A measure of the streamline curvature at the model is given by:-

$$\frac{\partial \bar{v}}{\partial x} = -I \lim_{z \to z_o} \left\{ \frac{d}{dz} \left[\frac{dw}{d\zeta} \frac{d\zeta}{dz} + \frac{i\Gamma}{2\pi} \frac{1}{(z - z_o)} \right] \right\} \qquad 4.5$$

where I means the imaginary part of. The solution in equation 4.3 and the transformation in equation 4.1 can be used in equations 4.4 and 4.5 to yield:-

$$\bar{u} = 0$$

$$\bar{v} = -\frac{\Gamma}{2h} \frac{\eta^2}{(\eta^2 + 1)^2} \qquad 4.6$$

$$\frac{\partial \bar{v}}{\partial x} = \frac{\pi\Gamma}{12h^2} \frac{(9\eta^4 - 10\eta^2 - 1)}{(\eta^2 + 1)^4} \qquad 4.7$$

The self-streamlining tunnel will have a >h and in some cases a>>h. With this condition an approximation to equation 4.2 is:-

$$\eta^2 \simeq \frac{2\pi a}{h} - 1 - \ln\left(\frac{2\pi a}{h} - 1\right)$$

which may be further simplified for present purposes to:-

$$\eta^2 \simeq \frac{2\pi a}{h}$$

Using this result, equations 4.6 and 4.7 become:-

$$\bar{v} \simeq -\frac{\Gamma}{4\pi a} \qquad 4.8$$

and

$$\frac{\partial \bar{v}}{\partial x} \simeq \frac{3\Gamma}{16\pi a^2} \qquad 4.9$$

Note that these results are independent of tunnel height h. If the model consists of a wing section of chord c and lift coefficient C_L in a free stream of velocity U, then the circulation Γ is given by:-

$$\Gamma = -\frac{1}{2} U c C_L \qquad 4.10$$

The upwash $\bar{v}$ can be interpreted as an incidence error $\bar{v}/U$ at the model and the corresponding lift coefficient error due to upwash ΔC_{LU} obtained from equations 4.8 and 4.10 as:-

$$\frac{\Delta C_{LU}}{C_L} \simeq \frac{1}{4}\frac{c}{a}\frac{a_1}{2\pi} \qquad 4.11$$

where a_1 is the section lift curve slope.

The streamline curvature $\frac{\partial \bar{v}}{\partial x}$ in equation 4.9 can be regarded as an equivalent parabolic camber for the aerofoil section, as shown in Fig.4.4. The equation for the camber line is:-

$$y_1 = 4r_c \frac{x_1(c - x_1)}{c}$$

whre r_c is the camber ratio. The velocity boundary condition at zero incidence is

$$\bar{v} \simeq - U \frac{dy_1}{dx_1}$$

Hence the curvature can be related to the camber ratio by:-

$$\frac{\partial \bar{v}}{\partial x} = \frac{\partial \bar{v}}{\partial x_1} = - U \frac{d^2 y_1}{dx_1^2} = 8 U \frac{r_c}{c} \qquad 4.12$$

Thin aerofoil theory shows that for a parabolic camber ratio r_c, the lift coefficient increment due to camber is

$$\Delta C_{LC} \simeq 2a_1 \dot{r}_c$$

Using equations 4.9, 4.10 and 4.12 this gives the lift coefficient error due to streamline curvature as:-

$$\frac{\Delta C_{LC}}{C_L} \simeq -\frac{3}{64}\left(\frac{c}{a}\right)^2 \frac{a_1}{2\pi} \qquad 4.13$$

Comparison of the results in equations 4.11 and 4.13 shows that for the normal case of wing chord c much smaller than the test section semi-length a, the upwash error is much the larger term.

4.2.2 Application of the interference analysis to choice of end sections

The results from the previous section are used with the configurations in Fig.4.1(a) and (b) by combining the contributions from both ends. For the solid/solid terminations the sense of the wall corrections is shown in Fig.4.5(a). When the model is located at mid-tunnel in both height and length, the upwash error ΔC_{LU} is zero because end contributions are equal in magnitude but of opposite senses. However, the contributions to stream curvature augment each other and the error ΔC_{LC} is twice that given by equation 4.13.

In the case of the solid/open jet ends the application is not as straightforward. It is known that, for lift interference,

the correction in a full open jet is twice that for a closed tunnel and opposite in sense. This characteristic is assumed to apply also to the case represented in Fig.4.5(b) where the jet interference vorticity is twice that of the solid wall vorticity and opposite in sense. This results in an upwash correction which is not only non-zero but is three times that given by equation 4.11. The curvature correction has the same magnitude as that of equation 4.13 but is of the opposite sign. Unfortunately, it is not clear how to deal with the open jet curvature produced by the model lift; for a full open jet tunnel this produces a downwash at the model which results in a correction of similar magnitude to that in equation 4.11. The situation is therefore unsatisfactory because corrections may be potentially large and it is not possible to predict what adjustable section length is necessary to reduce them to acceptable levels. With the University of Southampton tunnel used to date for interference-free tests, flow turning as in Fig.4.1(c) has been employed to minimise the uncertainty. The principle for determining the requirement of flow turning is illustrated in Fig.4.6. The model will produce an upwash component normal to the walls at A and B. An equivalent free stream flow U is conceived which makes an angle α_s to the tunnel centreline at entry in such a way that U $\sin\alpha_s$ exactly cancels the model upwash at A and B. The wall vorticity will be weak and tend to zero at A and B; the corresponding interference correction at the model will be small. The open jet vorticity is similarly small because the jet contour is also tangential to the streamlines at C and D. The datum line for the model

incidence and the streamline flow is the equivalent free stream flow direction at infinity, i.e. the line through the model and making an angle α_s with the tunnel centreline at inlet.

Whilst the interference for the tunnel with flow turning may be expected to be very small, it will not be zero because wall vorticity will develop upstream of A and downstream of C and the magnitude is again not easily assessed. A more promising arrangement would appear to be the solid/solid ends of Fig.4.1(b), with the virtues of:-

(a) zero upwash correction

(b) known curvature correction

(c) a layout easily realised in practice.

This layout is chosen as the basis for a study in the next section of the minimum length of adjustable section to give an acceptable interference level.

4.3 Solid/Solid Terminations and Section Length Criteria

This configuration lends itself to analysis using the complex z-plane representation in Fig.4.7(a). The plane is transformed to the upper half of the ζ-plane in Fig.4.7(b) by:-

$$\frac{\pi z}{h} = \frac{(\eta^2 - 1)}{2} \left(\frac{\zeta^2 - 1}{\zeta^2 - \eta^2}\right) + \ln \zeta \qquad 4.14$$

where the parameter η is related to the tunnel dimensions a and h by:-

$$\frac{\pi a}{h} = \frac{(\eta^4 - 1)}{4\eta^2} + \ln \eta \qquad 4.15$$

The relationship is illustrated in Fig.4.8. The limit a = 0 (η = 1) represents the closed tunnel case.

The complex potential in the ζ-plane for a vortex Γ at P is exactly the same as that in equation 4.3 and the formal expressions for the velocity components $\bar{u}$, $\bar{v}$ and the curvature $\frac{\partial \bar{v}}{\partial x}$ are as given in equations 4.4 and 4.5.

Using $z_o = a + ih/2$ and the transformation in equation 4.14, equations 4.4 and 4.5 give:-

$$\bar{u} = 0 \qquad \bar{v} = 0$$

$$\frac{\partial \bar{v}}{\partial x} = \frac{4\pi\Gamma}{3h^2} \frac{\eta^4}{(\eta^2 + 1)^6} (3\eta^4 - 10\eta^2 + 3)$$

These results confirm that there is no upwash interference at the model and only flow curvature is present. The equivalent parabolic camber concept can be applied as before to the curvature to give the resultant lift coefficient error ΔC_{LC} as:-

$$\frac{\Delta C_{LC}}{C_L} = -\left(\frac{c}{h}\right)^2 \frac{a_1}{2\pi} f(\eta) \qquad 4.16$$

where

$$f(\eta) = \frac{\pi^2}{3} \frac{\eta^4}{(\eta^2 + 1)^6} (3\eta^4 - 10\eta^2 + 3) \qquad 4.17$$

This result can be used to determine acceptable tunnel lengths for engineering purposes by assuming $a_1 \simeq 2\pi$ and plotting in the form of the interference or error parameter $\frac{\Delta C_{LC}}{C_L} \left(\frac{h}{c}\right)^2$ shown in Fig.4.9.

For a chord/height ratio of unity, this parameter is a direct measure of lift coefficient error. The closed tunnel case of a = 0 gives an error of 20.6%. This falls rapidly with increasing length of streamline section and for a semi-length/height ratio of about 0.35 there is zero correction. With a length/height ratio of about 2, the error reaches a maximum negative value of about 4.3%. For length/height ratios in excess of 5 the error is less than 1%. The apparent advantage of using a relatively short flexible section is probably illusory for the following reasons:-

1) If the section length 2a is of the same order as the chord c and tunnel height h, the lift representation as a concentrated vortex is not reasonable. Thus, whilst the overall lift correction may still not be large, the pressure distribution may be significantly in error, and pressure gradients and boundary layer development or separation may be unrepresentative.

2) The error parameter is very sensitive to a/h for small values of a/h and there is a problem in practice in determining an effective value for a. A possible interpretation is illustrated diagrammatically in Fig.4.10. With the flow and circulation senses shown, the present correction theory would produce stagnation points on the upper faces of the slits although

only a small fraction of tunnel height away from the ends. There would be local distortions compared with the fully free streamline but allowances could be made for this in determining the correct setting for the first jack. The fairing sections reduce the effective length of correctly streamlined wall but the value of $^{a}/_{h}$ may be taken as that corresponding to the distance between first and last jacks.

It is therefore felt that if these factors are to be removed and a tunnel correction of less than 1% is reasonable, then a section length/height ratio greater than 5 is required at low (incompressible) tunnel speeds.

The upwash error or correction is eliminated because of the symmetric positioning of the model lift centre relative to the solid ends, as indicated in Fig.4.11. Note that the model will not in general be central with respect to the flexible wall section. Errors can therefore result from the following:-

1) Model lift centre may not be known accurately beforehand and there may be an effective model offset.

2) The model will have finite size although chord/tunnel length ratios can be kept reasonable.

3) The model will in general have a pitching moment.

These factors need more detailed work but preliminary study has shown them to produce effects an order less than the curvature correction derived here.

For completeness, consideration must also be given to solid and wake blockage corrections. However, consideration of the fundamental representation of solid blockage by a doublet,

whose velocity disturbance is varying as the square of the distance, shows that the vortex lift case is more critical. The symmetric arrangement again helps in minimising the wake blockage error but since this is a source term, the magnitude could be of the same order as (but no larger than) the lift correction. It is therefore anticipated that the criteria for the termination of the tunnel flexible section are adequate for all corrections.

4.4 Compressibility Effects at Moderate Tunnel Mach Numbers

For tunnel Mach numbers below that for critical flow at the model, some measure of the effect of compressibility may be obtained by applying the subsonic similarity rule to the result in equation 4.16. To simplify the process without losing practical relevance, it is assumed that $^{a}/_{h}$ is significantly greater than 1 and that equations 4.15 and 4.17 can be replaced by the approximate forms:-

$$\frac{\pi a}{h} = \frac{\eta^2}{4} \qquad 4.15a$$

$$f(\eta) = \frac{\pi^2}{\eta^4} = \frac{1}{16}\left(\frac{h}{a}\right)^2 \qquad 4.17a$$

Equation 4.16 then reduces to:-

$$\frac{\Delta C_{LC}}{C_L} = -\frac{1}{16}\left(\frac{c}{a}\right)^2 \frac{a_1}{2\pi} \qquad 4.16a$$

i.e. the correction is independent of tunnel height. Now ΔC_{LC} and C_L vary in the same way with Mach number M, and c and a are both measured in the stream direction. The only variation is therefore through the section lift curve slope which increases as $(1 - M^2)^{-\frac{1}{2}}$. Using the subscripts I for incompressible and C for compressible flow, equation 4.16a gives for the same tunnel geometry:-

$$\left(\frac{\Delta C_{LC}}{C_L}\right)_C = \frac{1}{\sqrt{1 - M^2}} \left(\frac{\Delta C_{LC}}{C_L}\right)_I$$

Alternatively, for the same lift coefficient ratio and the same model chord, the tunnel semi-length/height ratio have to be increased in the form:-

$$\left(\frac{a}{h}\right)_C = \frac{1}{4\sqrt{1 - M^2}} \left(\frac{a}{h}\right)_I$$

This is illustrated in Fig.4.12 for C = h and a 1% value for $\Delta C_{LC}/C_L$. The required tunnel length increases with Mach number but only slowly over the range shown. Even at M = 0.8, a 30% longer tunnel would give the same interference level. Above M = 0.8, the argument is invalid because the similarity rule will break down in this transonic regime and a more sophisticated analysis would be needed.

5. A PREDICTIVE METHOD FOR RAPID WALL ADJUSTMENT

5.1 Basis of the Method

In order to improve the rate of convergence of the source method used to date with the low speed tunnel[1,2], an alternative process has been sought. The basic steps in this process are:-

(1) For a given distribution of measured wall static pressure, the flow velocity internally at the wall can be determined.

(2) For a given wall shape, the external imaginary flow field can be calculated theoretically.

(3) The velocity jump across the wall obtained from the values in (1) and (2) is a direct measure of a notional vorticity distribution at the wall. Moreover, this vorticity distribution has the characteristic that the velocity component induced normal to the wall just cancels the sum of the normal components of velocity due to the model and the undisturbed free stream.

(4) The strategy for wall adjustments is one in which the local wall slope is modified until the freestream component normal to the wall just balances the model component. The wall vorticity is then zero. The wall co-ordinates are determined by integration of the wall slope distribution.

An iteration process would still be required because the model flow may be modified by the wall movement but it is anticipated that convergence is rapid. As shown in the subsequent sections, it is unnecessary to perform step (2) explicitly if a suitable

starting point and iteration process are adopted. In order to afford a simple analytic illustration of the method, the case of a single wall adjustment is taken in the next section.

5.2 Illustration of the Adjustment Process

A simple formulation can be obtained from the consideration of a two-dimensional model near a doubly infinite flat plate representing the upper wall of a two-dimensional tunnel. The flat plate is taken as the starting point because the imaginary external flow field is the simple one of uniform flow at the undisturbed tunnel speed U. The situation is shown in Fig.5.1. The subscript O indicates the initial arrangement and the origin of the x, y-coordinates is a suitable fixed reference point in the wall structure. The velocity increment $u_o(x)$ is determined from the wall static pressure distribution. The velocity components $u_{mo}(x)$ and $v_{mo}(x)$ are the increments over free stream produced by the model in an infinite flow field. It can readily be seen that the vorticity $\gamma_o(x)$ is given by:-

$$\gamma_o(x) = u_o(x) \qquad 5.1$$

that the model velocity component is:-

$$u_{mo}(x) = \tfrac{1}{2}\, u_o(x) \qquad 5.2$$

and that the horizontal velocity component of the flow without wall interference is given by:-

$$U + u_{mo}(x) = U + \tfrac{1}{2} u_o(x) \qquad 5.3$$

For the infinite wall shown in Fig.5.1, the condition of zero penetration at the solid surface results in the relationship:-

$$v_{mo}(x) - \frac{1}{2\pi} \int_{-\infty}^{+\infty} \frac{\gamma_o(\xi)}{(\xi - x)} \, d\xi = 0 \qquad 5.4$$

This result can be used to determine the modified wall shape $y_1(x)$ as shown in Fig.5.2. The approximate normal velocity condition is:-

$$[U + u_{mo}(x)] \frac{dy_1}{dx} = v_{mo} \qquad 5.5$$

Approximations are present because the slope is assumed everywhere to be small and also because the distribution $u_{mo}(x)$ is correct only at the original wall location ($y = 0$). In practice, it is unlikely these will give significant errors. Equations 5.1, 5.3, 5.4 and 5.5 can be combined to give:-

$$[U + \tfrac{1}{2}u_o(x)] \frac{dy_1}{dx} = \frac{1}{2\pi} \int_{-\infty}^{+\infty} \frac{u_o(\xi)}{(\xi - x)} d\xi \qquad 5.6$$

The slope can therefore be determined directly from the measured quantity $u_o(x)$. Care must be taken in the numerical evaluation

of the integral in equation 5.6 particularly in the region of the singularity $\xi = x$. A principal value interpretation must be used and this is achieved by a local analytic fit to the data in the form of a polynomial in ξ and piecewise analytic integration. The numerical integration of the slope to give the wall coordinates is straightforward. It is anticipated that a large proportion of the total wall adjustment will be accomplished through y_1.

5.3 Starting Point for the Second Wall Adjustment

For a second application of the adjustment process, the wall can be moved to $y_1(x)$ and the new wall static pressure distribution measured. The external imaginary flow is no longer uniform and must, in principle, be calculated for the given shape $y_1(x)$. The normal velocity boundary condition for the flow U over such a shape is:-

$$U \frac{dy_1}{dx} = - \frac{1}{2\pi} \int_{-\infty}^{+\infty} \frac{\gamma_{w1}(\xi)}{(\xi - x)} \, d\xi \qquad 5.7$$

where $\gamma_{w1}(x)$ is the distribution of surface vorticity. Comparison of equations 5.7 and 5.6 shows that, provided u_o is everywhere small compared with U, the following approximation holds:-

$$\gamma_{w1}(x) = -u_o(x)$$

and the flow over the upper surface of the wall is given by:-

$$U - \tfrac{1}{2}\gamma_{w1}(x) = U + \tfrac{1}{2}u_o(x) \qquad 5.8$$

Equation 5.8 therefore shows that, provided the first wall adjustment is made according to the method in Section 5.2, the external flow for the second adjustment can be obtained directly from the measured internal velocity used for the first adjustment.

5.4 General Application of Process

The process of Sections 5.2 and 5.3 can be generalised to any order of iteration and it is always possible to relate the external flow field for one adjustment to the measured internal velocity of the previous adjustment. Account of both tunnel walls can be taken by applying the adjustment process to each independently and regarding their mutual interference as part of the model flow change. Alternatively, since the vorticity distributions of both walls are always known, it would be possible to include both in a modified form of equation 5.4. However, computational complexity and run times would increase and iteration would not be avoided, because of model flow adjustment resulting from wall movement.

Tunnel length considerations mean that the integrals in equations 5.4, 5.6 and 5.7 have finite limits but, in conjunction with the layout arguments of Chapter 4, it is not anticipated that this will present a significant error. Wall boundary layer growth can be incorporated where necessary as in the present technique and an error measure for termination of the iteration process can be developed from a root mean square change of wall position from one iteration to the next or from an equivalent velocity/ pressure parameter.

6. CONCLUSIONS

1. A method has been developed for accurately computing the imaginary flowfields outside a flexible walled test section, applicable to lifting and non-lifting models.

2. The tolerances in the setting of the flexible walls introduce only small levels of aerodynamic interference at the model. While it is not possible to apply corrections for the interference effects, they may be reduced by improving the setting accuracy of the portions of wall immediately above and below the model.

3. Interference effects of the truncation of the length of the streamlined portion of a test section can be brought to an acceptably small level by the use of a suitably long test section with the model placed centrally, but the required length is not impractical.

4. A method for rapidly converging the walls to the desired streamline shapes is proposed. Experimental work is required to confirm predictions.

SYMBOLS

a	Tunnel working section semi-length
a_1	Two-dimensional lift curve slope
c	Wing chord
$C_L, \Delta C_{LU}, \Delta C_{LC}$	Lift coefficients
C_p	Pressure coefficient
d	Length of wall bump
$f(\eta)$	Function defined by equation 4.17
h	Tunnel working section height
M	Mach number
$m(x)$	Source strength per unit length of wall
N, n	Indices
P_n	Probability
r_c	Camber ratio
t	Wall setting tolerance
$U, u, v, \bar{u}, \bar{v}$	Velocity components
w	Complex potential ($w = \phi + i\psi$)
$x, y; x_1, y_1$	Coordinates
x_b	Coordinate of the nose of the wall bump relative to the wing quarter chord
Δy	Wall movement relative to the straight
z, z_o	Complex variables ($z = x + iy$)
α_s	Flow turning angle
Γ	Vortex strength
γ_o, γ_{wl}	Wall vorticity distributions
η	Transformation parameter
ξ	Dummy variable

ϕ	Velocity potential
ψ	Stream function

Suffix

I	Incompressible
C	Compressible

REFERENCES

1. M.J. Goodyer — "The Self Streamlining Wind Tunnel" NASA TMX-72699, August 1975

2. M.J. Goodyer — "A Low Speed Self-Streamlining Wind Tunnel" AGARD Conference Proceedings No.174 - Wind Tunnel Design and Testing Techniques, London, October 1975

3. W.J. Duncan, A.S. Thom, and A.D. Young — "Mechanics of Fluids" Published by Arnold

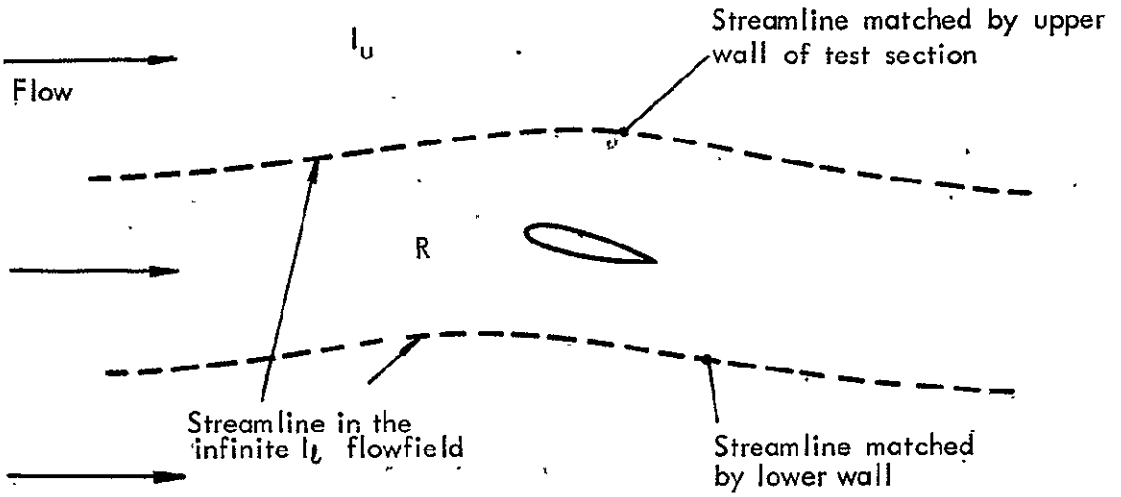

FIG. 2.1. DIVISION OF THE INFINITE TWO DIMENSIONAL FLOWFIELD BY FLEXIBLE TEST SECTION WALLS INTO ONE REAL R AND TWO IMAGINARY PARTS I_u AND I_ℓ

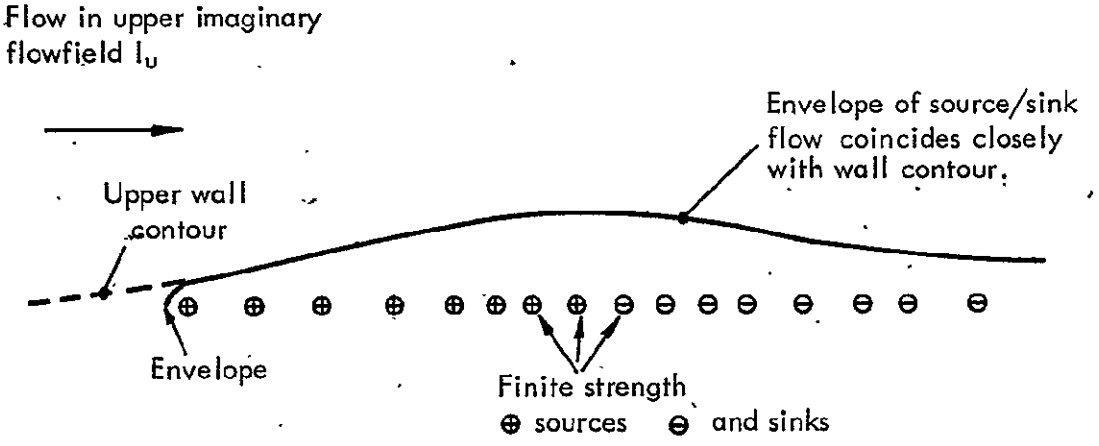

FIG. 2.2. MATHEMATICAL MODEL REPRESENTING THE UPPER IMAGINARY FLOWFIELD.

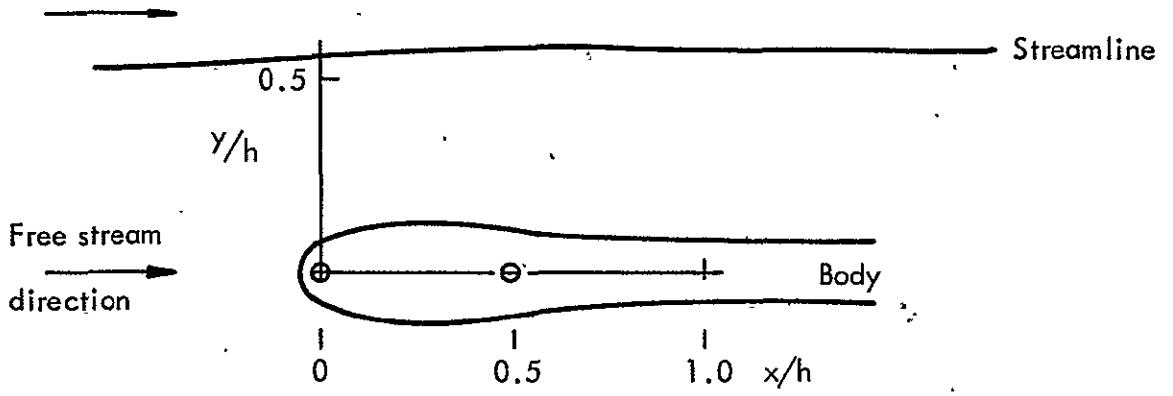

FIG. 2.3. A NON-LIFTING SOURCE/SINK BODY AND AN ADJACENT STREAMLINE AT THE POSITION OF A FLEXIBLE WALL.

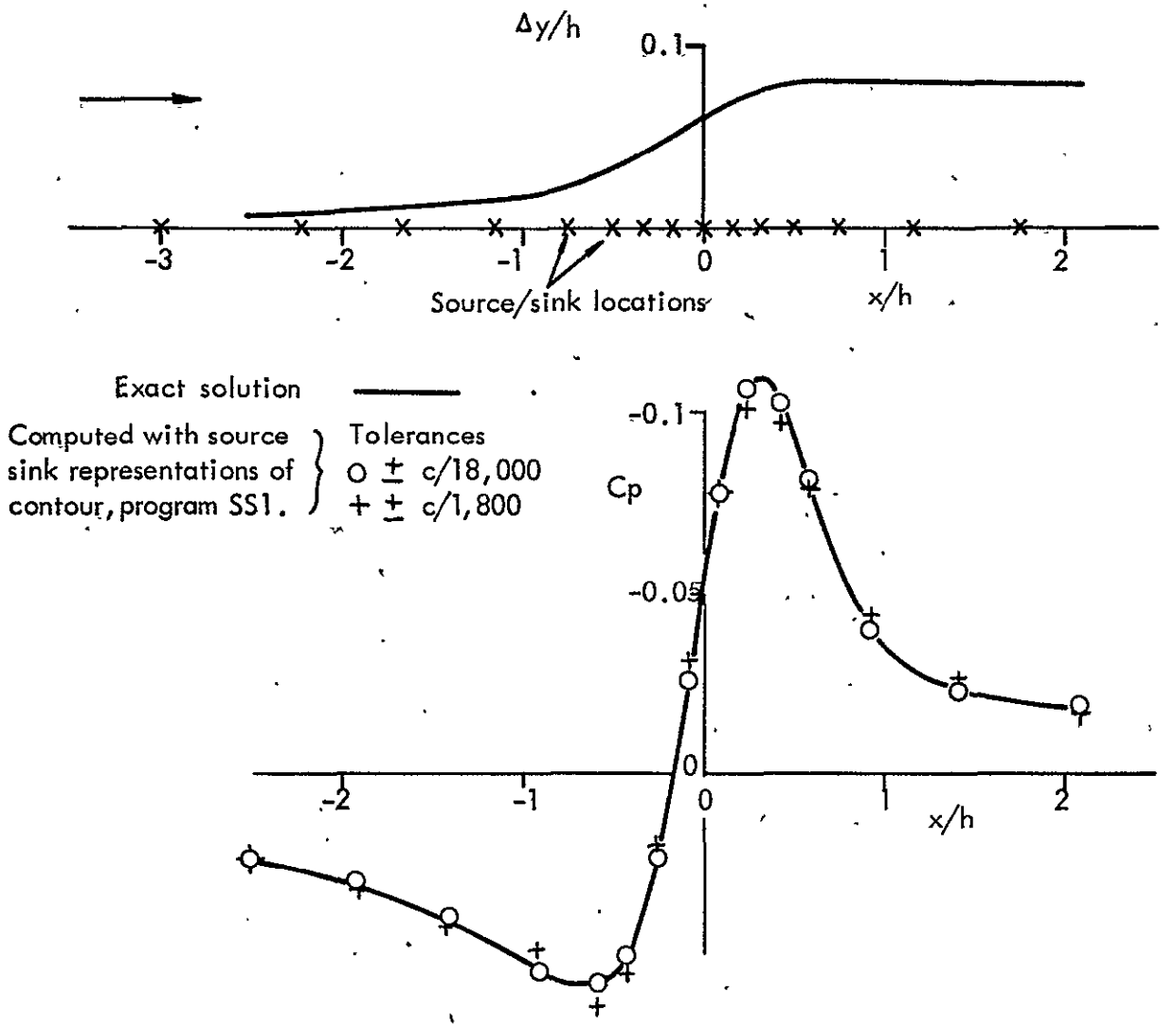

FIG. 2.4. THE TEST SECTION WALL CONTOUR WITH WALL SOURCE/SINK LOCATIONS, AND PRESSURE DISTRIBUTIONS.

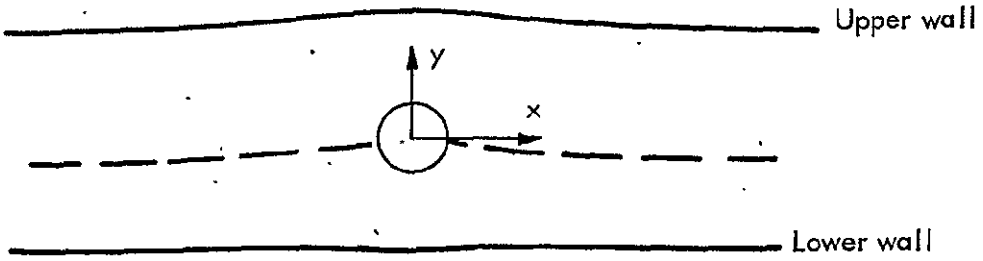

FIG. 2.5. A LIFTING CYLINDER IN AN INFINITE FLOWFIELD, WITH A PAIR OF STREAMLINES REPRESENTING TEST SECTION WALLS.

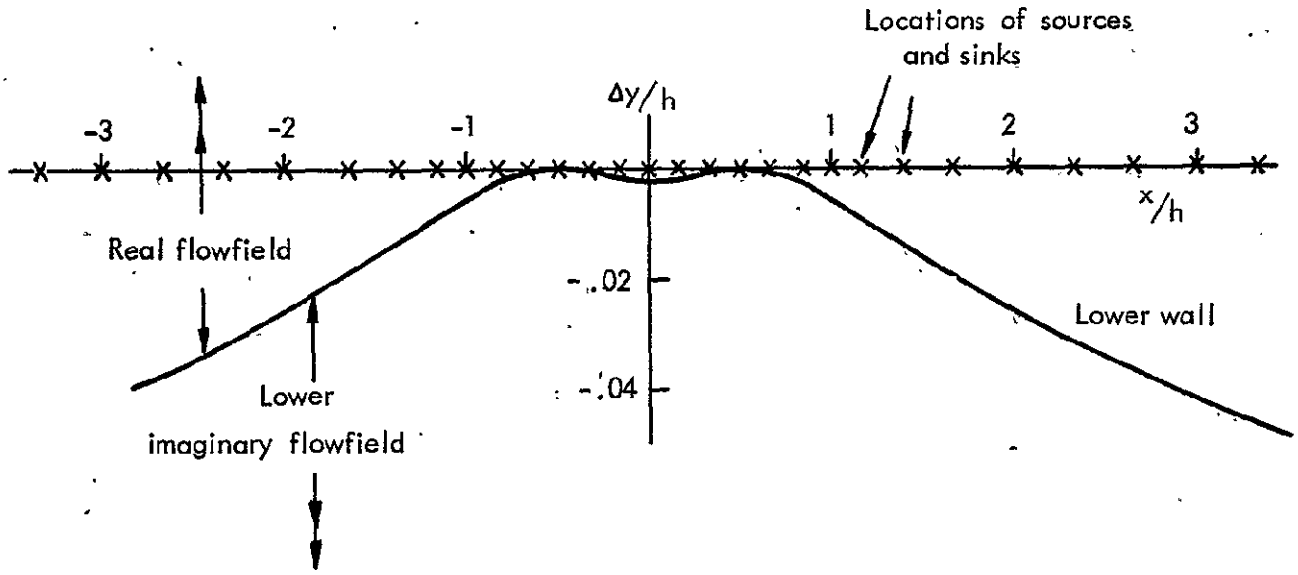

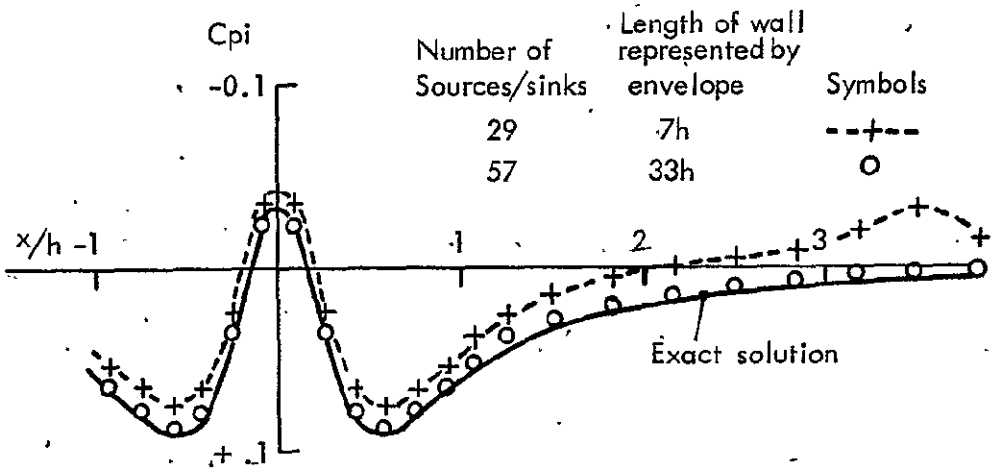

FIG. 2.6. THE CONTOUR OF THE LOWER TEST SECTION WALL STREAMLINED AROUND A LIFTING CYLINDER, TOGETHER WITH COMPARISONS OF THE EXACT WALL PRESSURE DISTRIBUTION WITH DISTRIBUTIONS GIVEN BY PROGRAM SS1 FOR THE LOWER IMAGINARY FLOWFIELD.

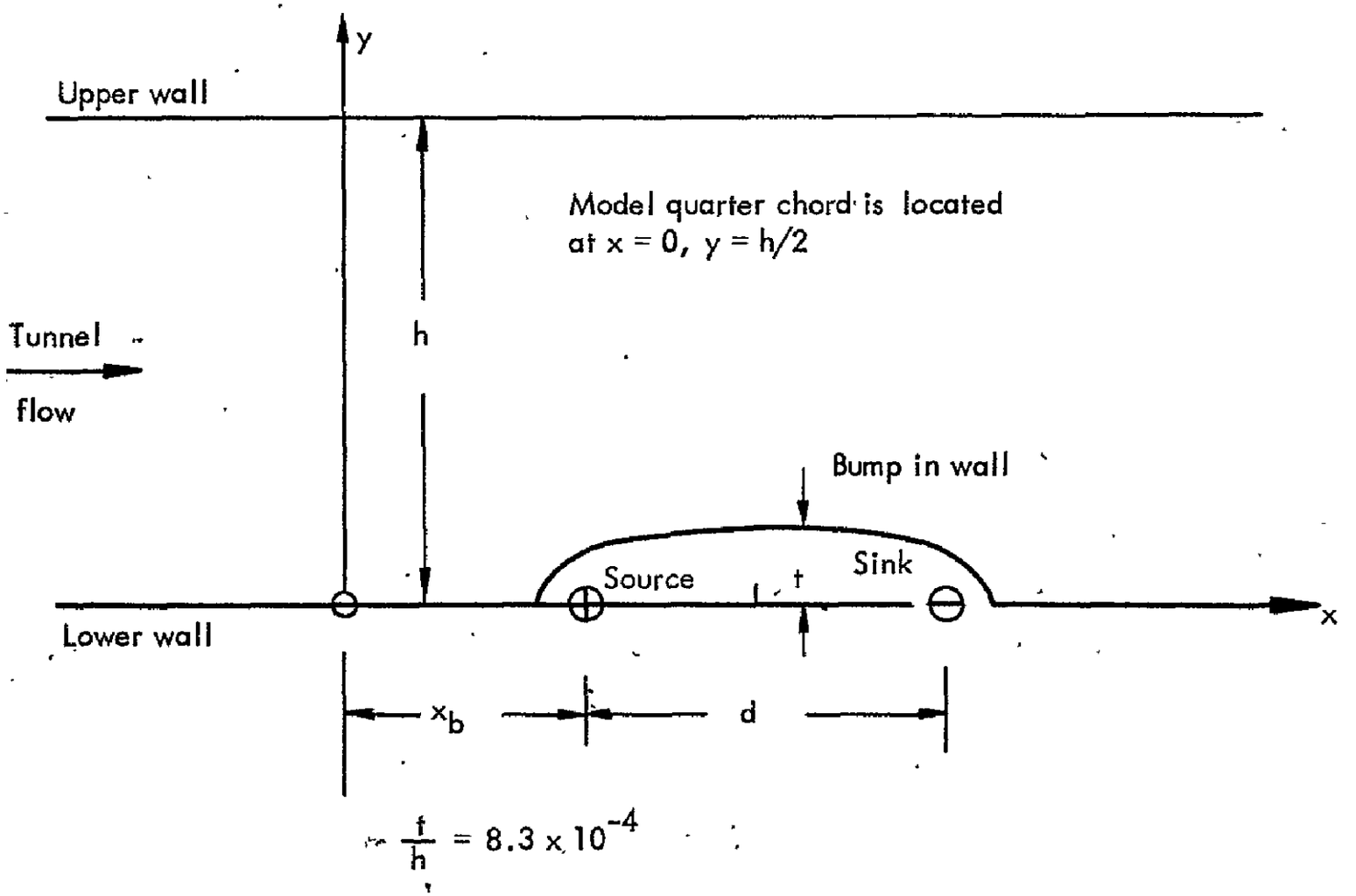

FIG. 3.1. TEST SECTION STREAMLINES TO REPRESENT JACK POSITION ERROR.

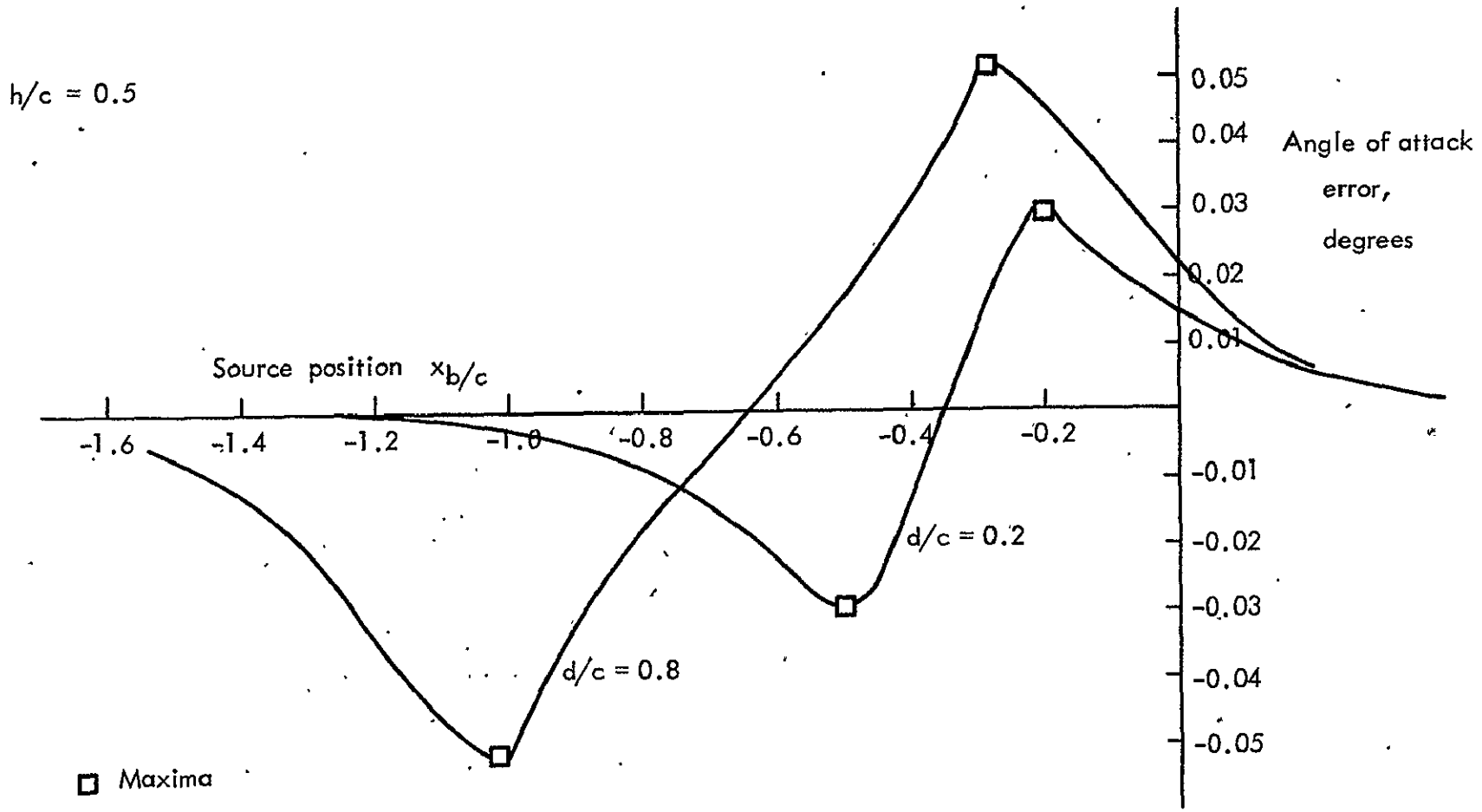

FIG. 3.2a. ANGLE OF ATTACK ERROR AS A FUNCTION OF BUMP POSITION.

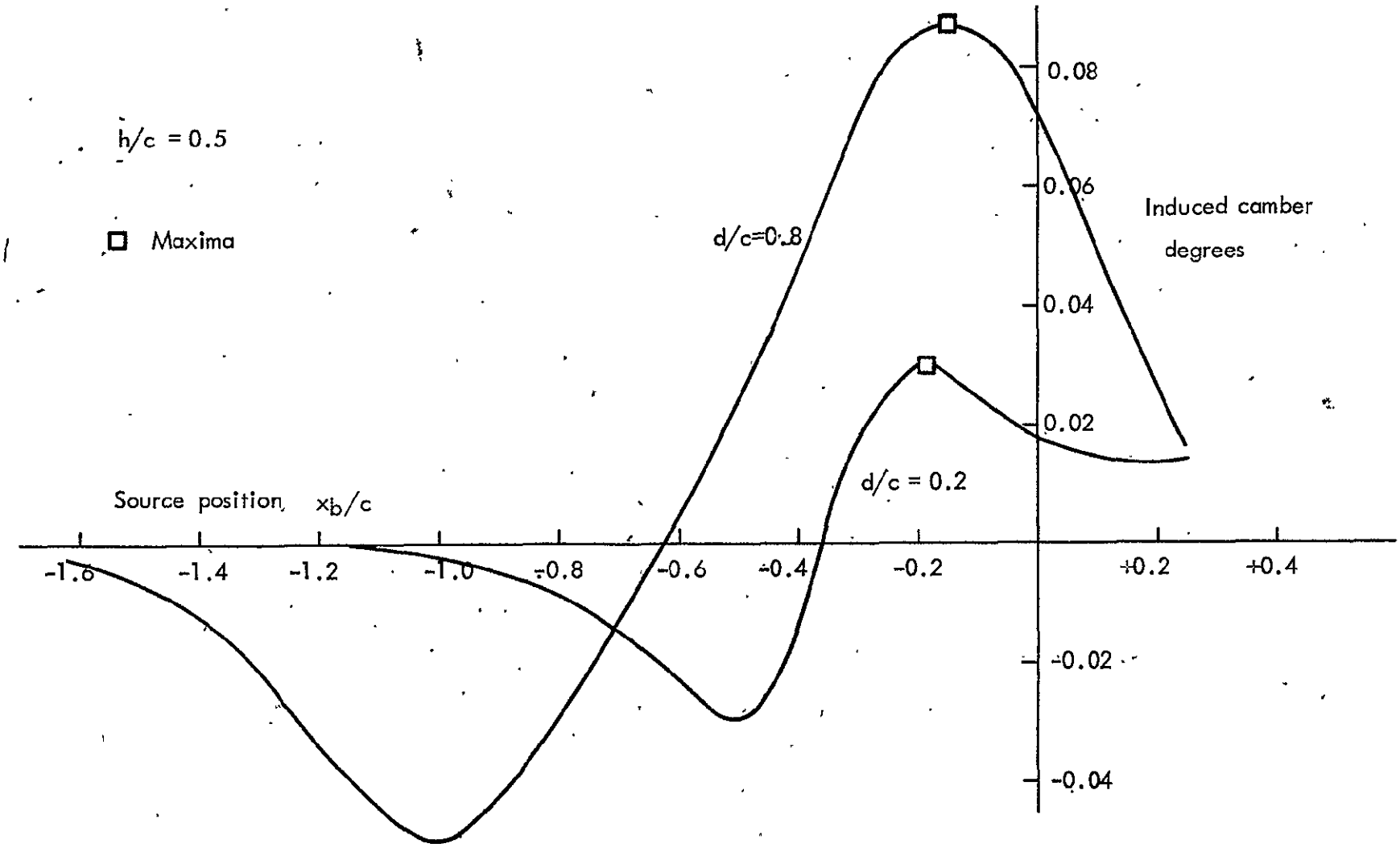

FIG. 3.2b. INDUCED CAMBER AS A FUNCTION OF BUMP POSITION.

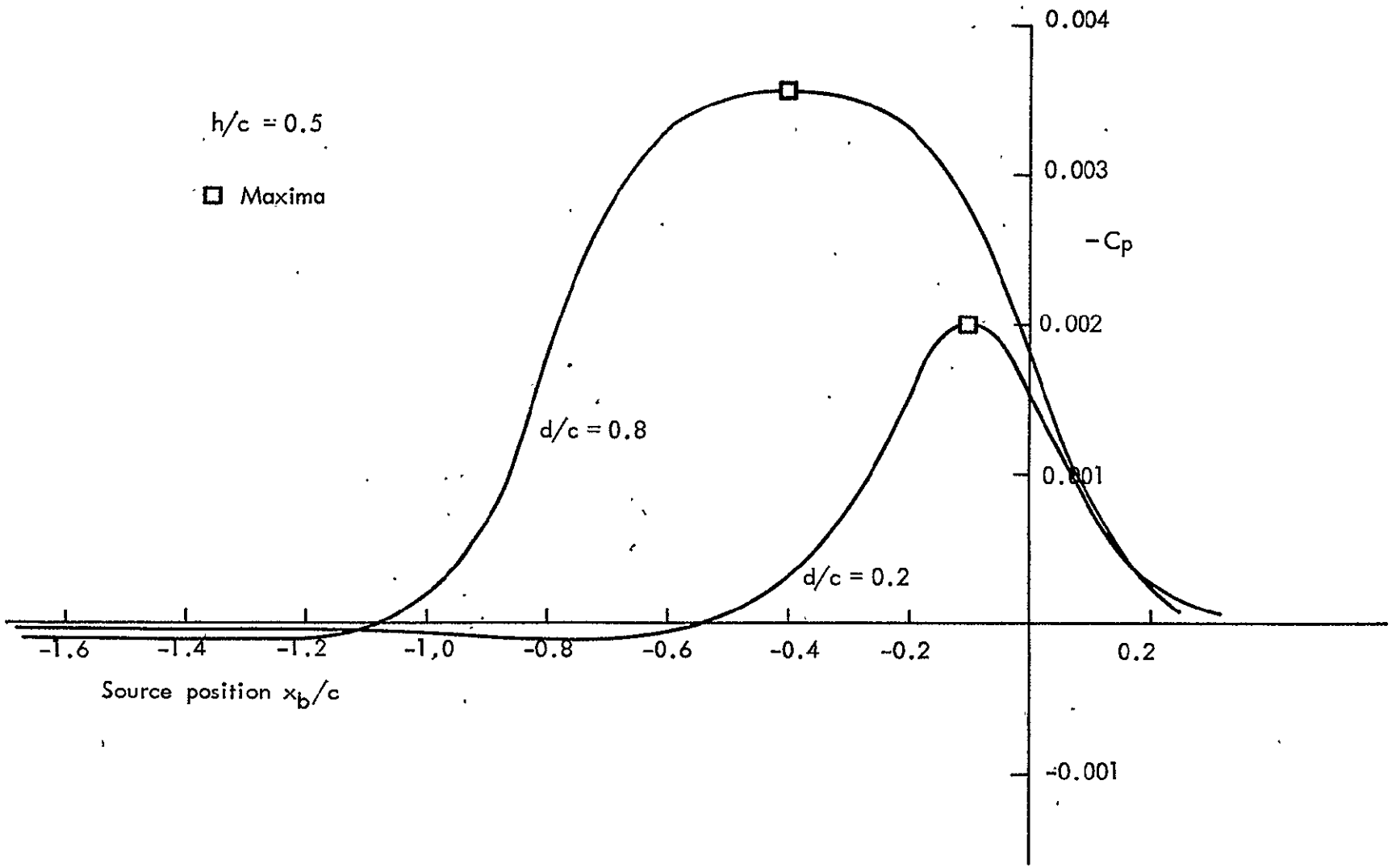

FIG. 3.2c. PRESSURE COEFFICIENT ERROR AS A FUNCTION OF BUMP POSITION.

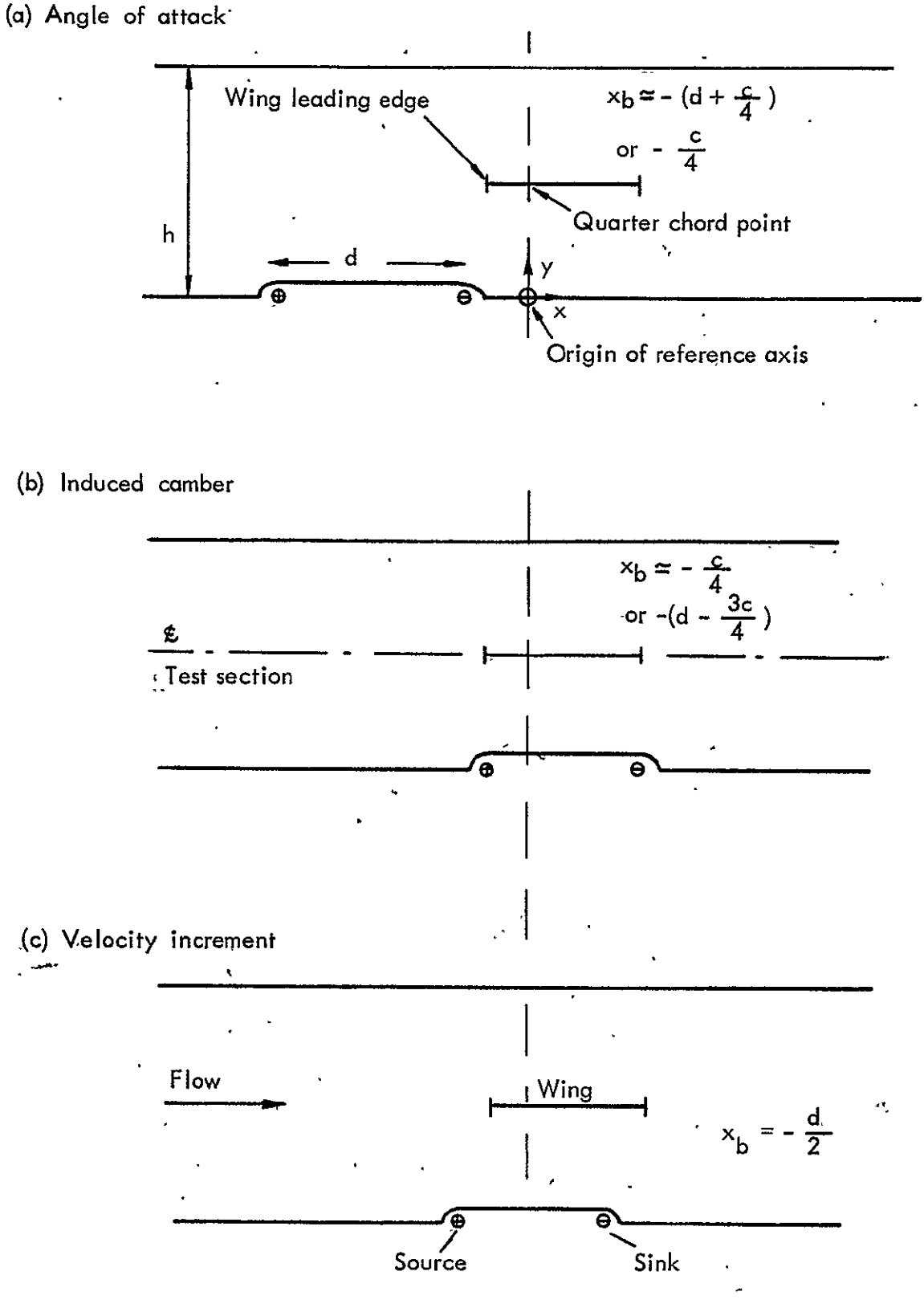

FIG. 3.3. BUMP POSITIONS FOR MAXIMUM INTERFERENCES.

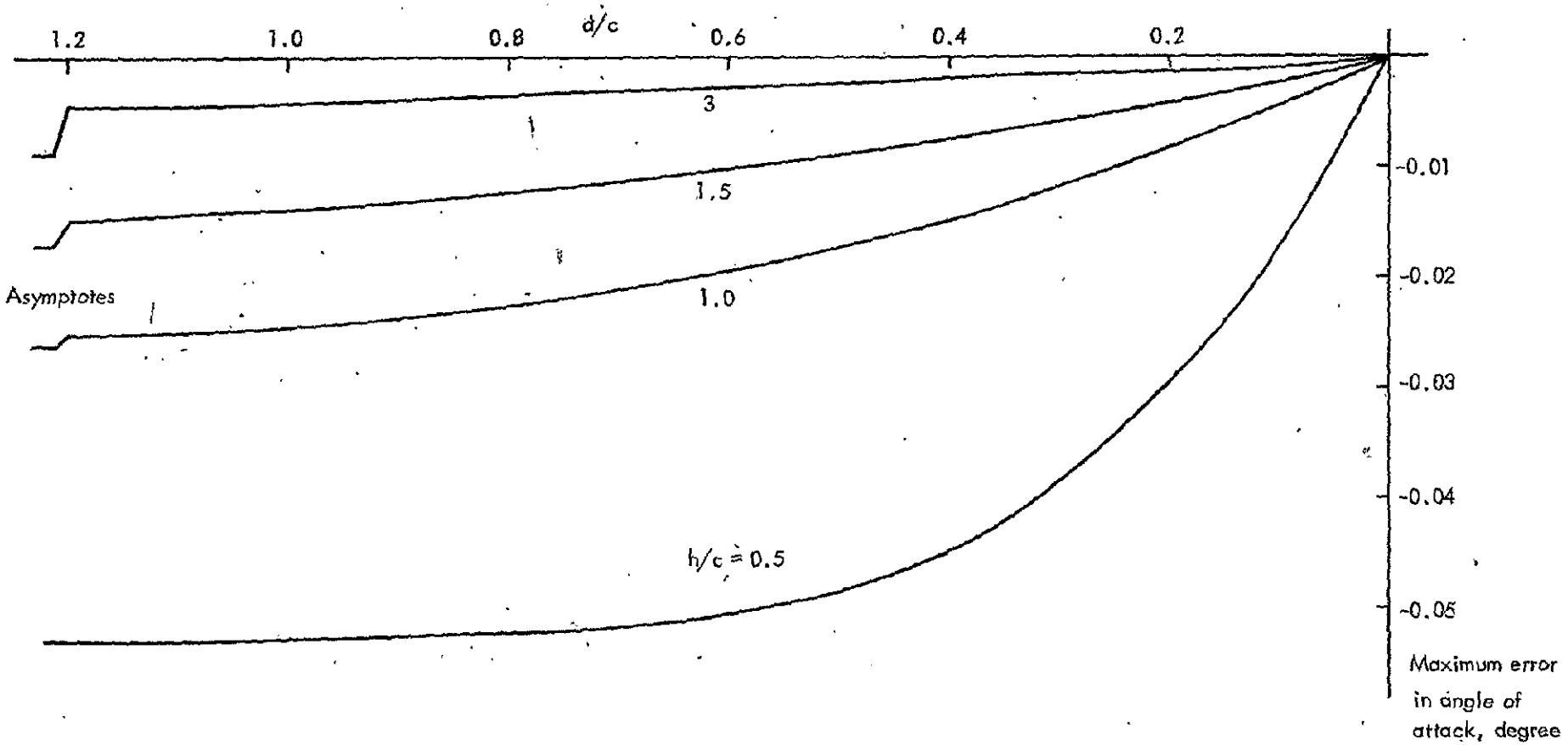

FIG. 3.4a. MAXIMUM ANGLE OF ATTACK INTERFERENCE AS A FUNCTION OF BUMP LENGTH.

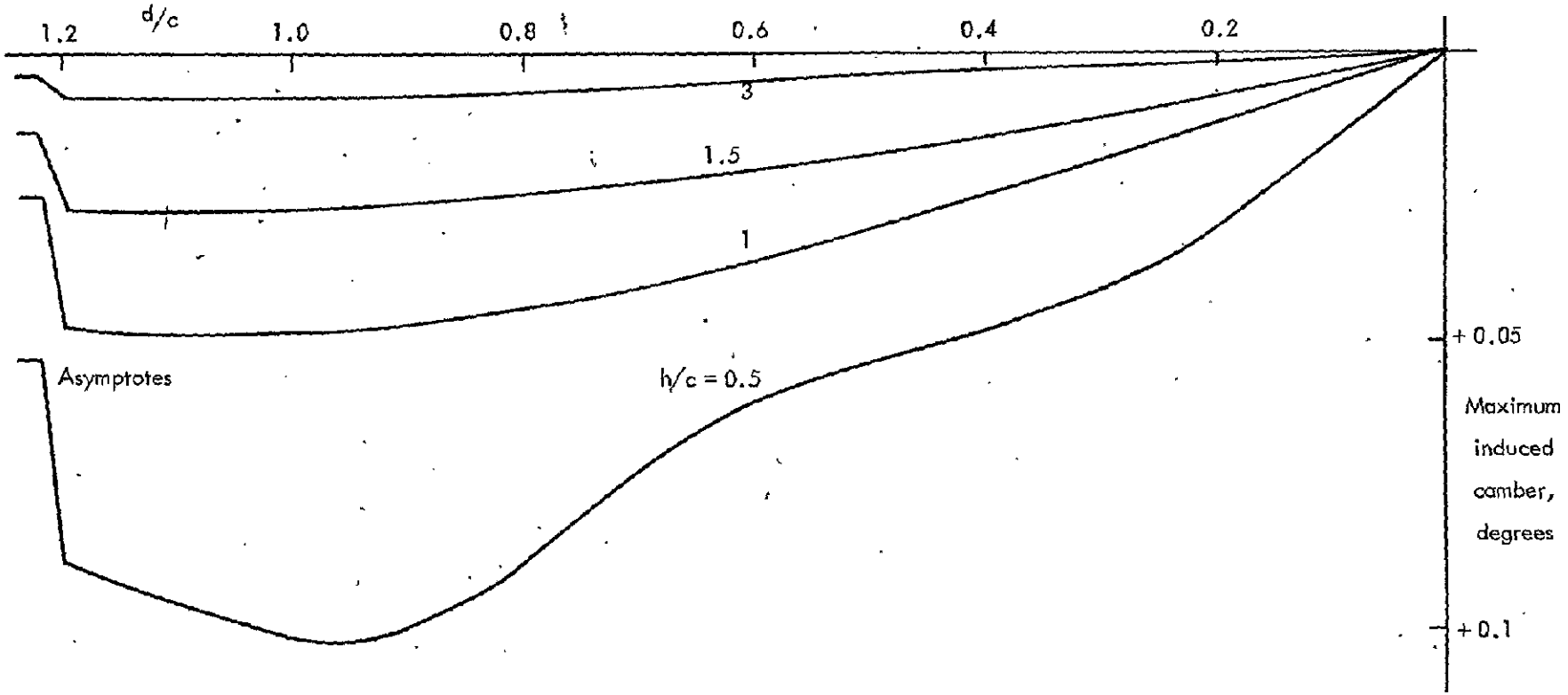

FIG. 3.4b. MAXIMUM INDUCED CAMBER INTERFERENCE AS A FUNCTION OF BUMP LENGTH.

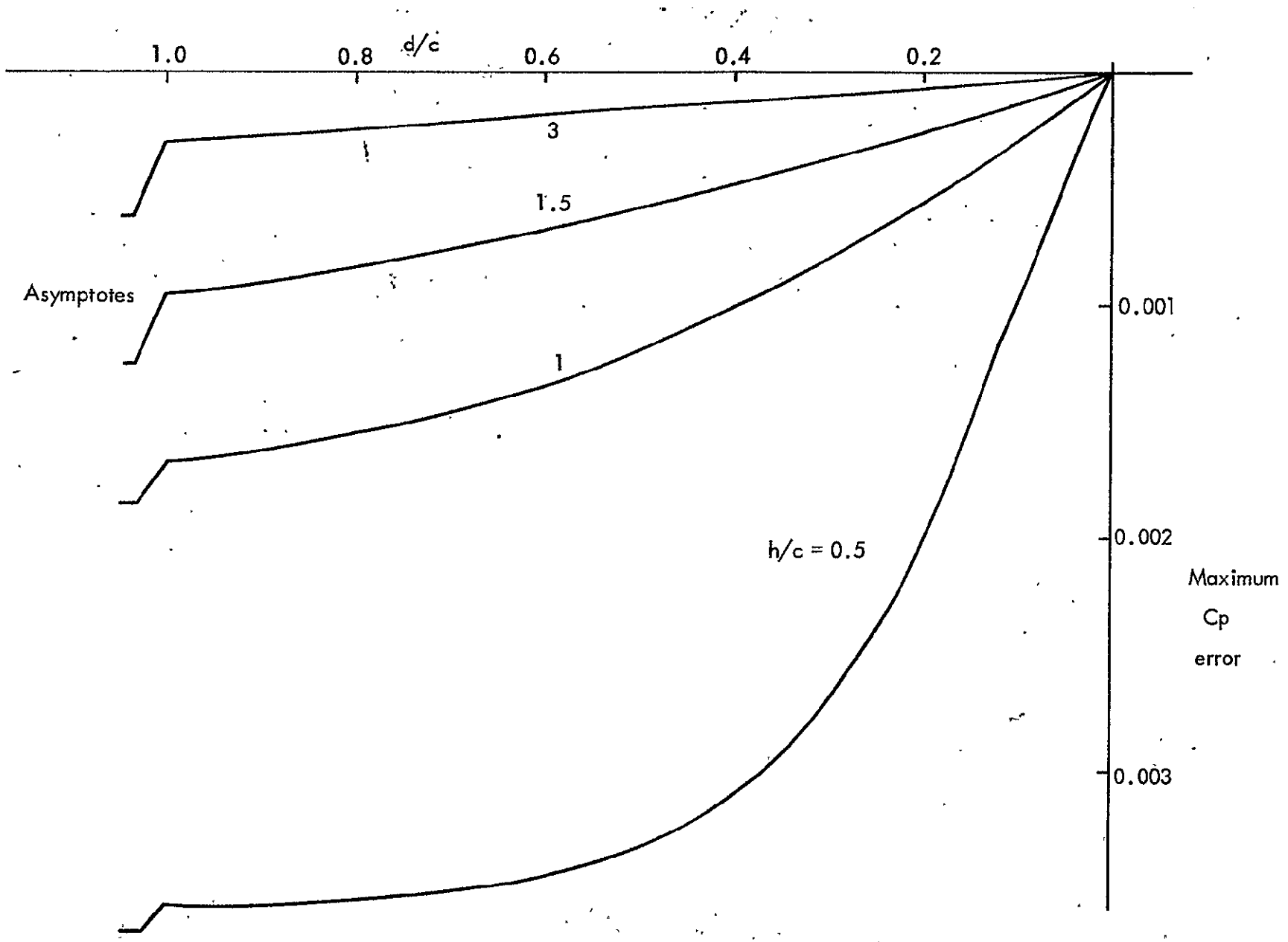

FIG. 3.4c. MAXIMUM PRESSURE COEFFICIENT ERROR AS A FUNCTION OF BUMP LENGTH.

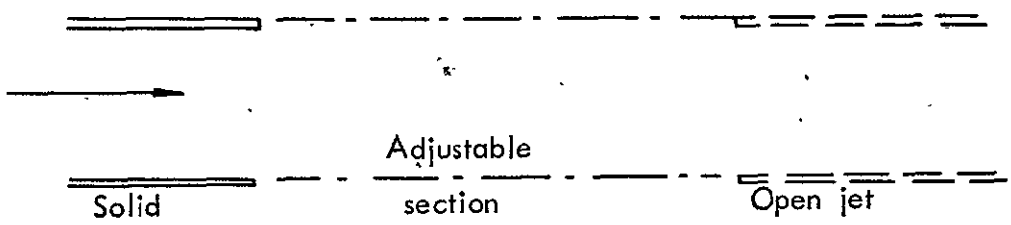

a) Solid / open jet terminations

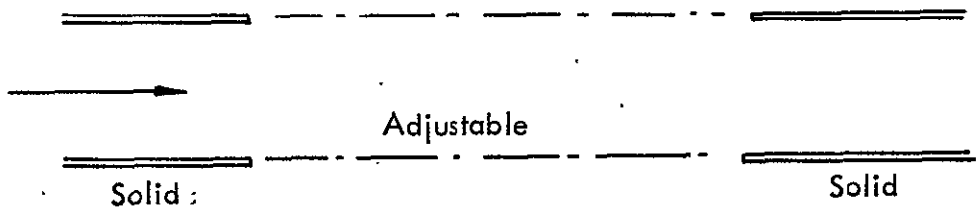

b) Solid/solid terminations.

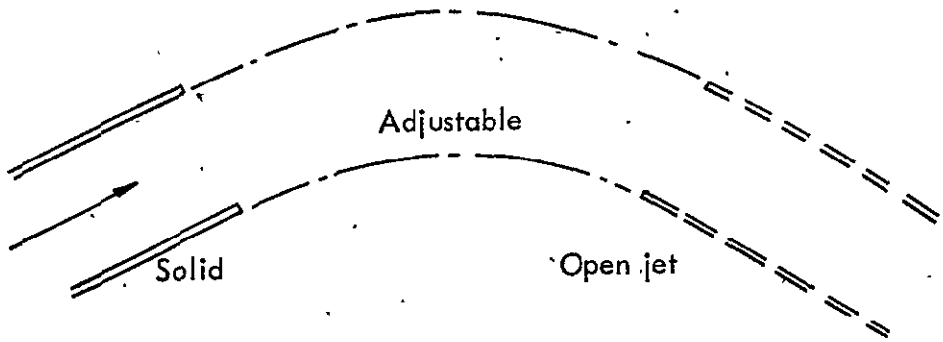

c) Solid/open jet terminations with flow turning.

FIG. 4.1. TERMINAL CONFIGURATIONS.

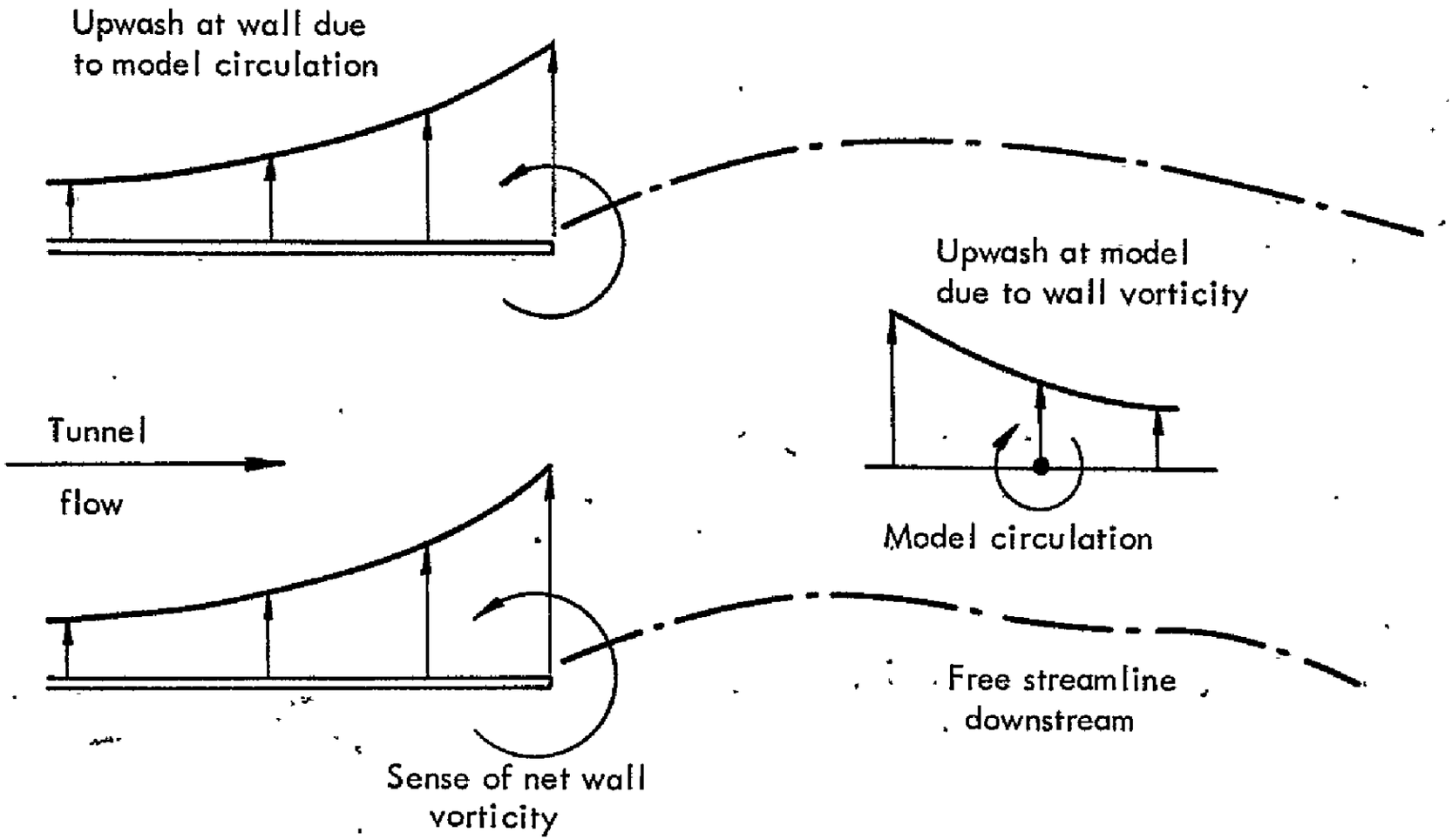

FIG. 4.2. BASIC CASE.

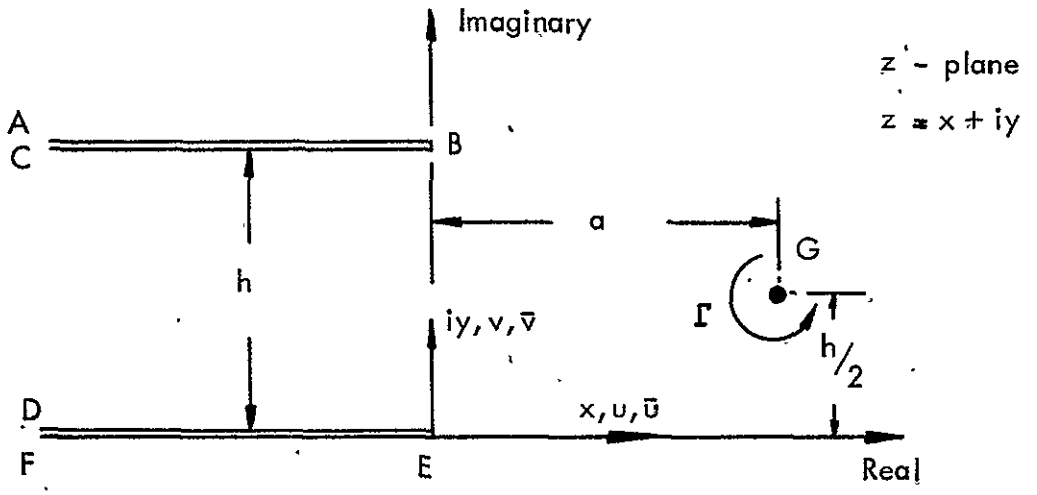

(a) Complex z - plane.

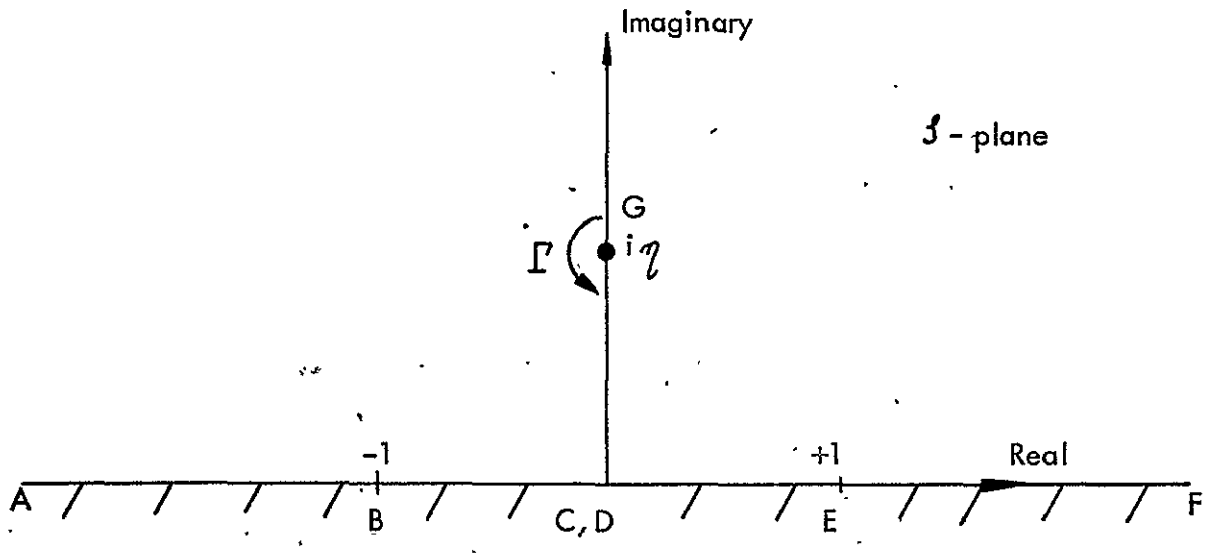

(b) Transformed ζ - plane

FIG. 4.3. PHYSICAL AND TRANSFORMED PLANES.

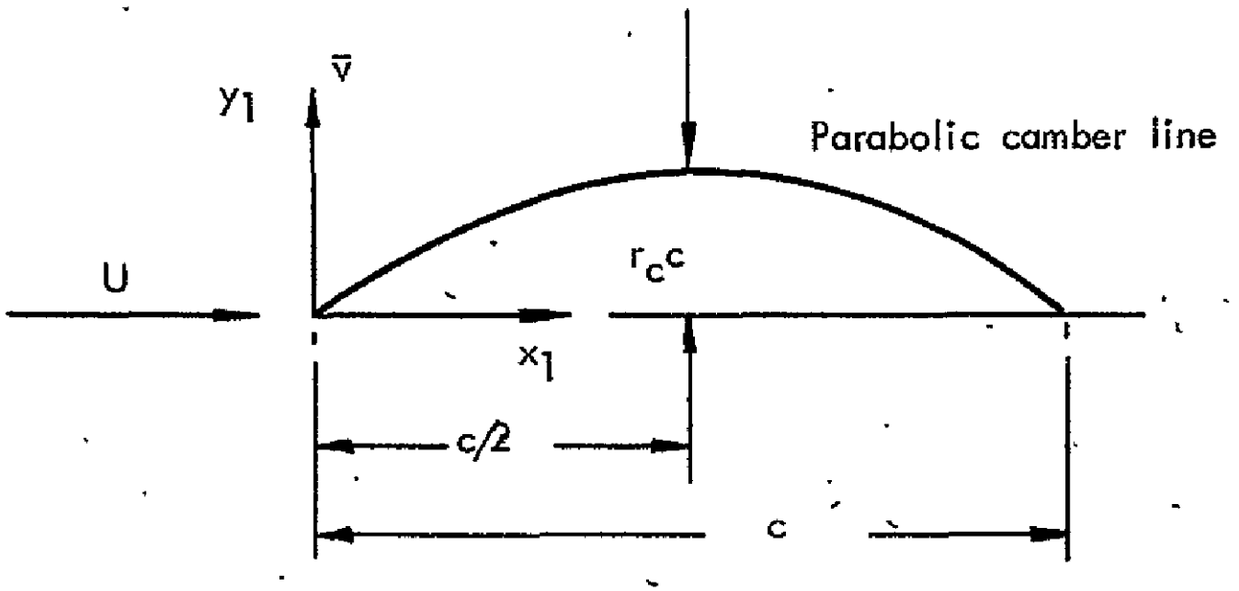

FIG. 4.4. PARABOLIC CAMBER LINE.

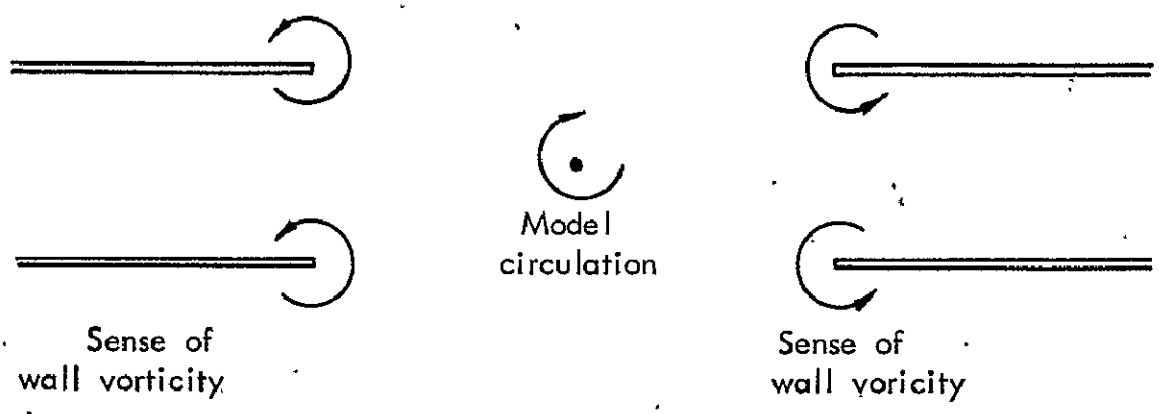

a) Solid/solid terminations.

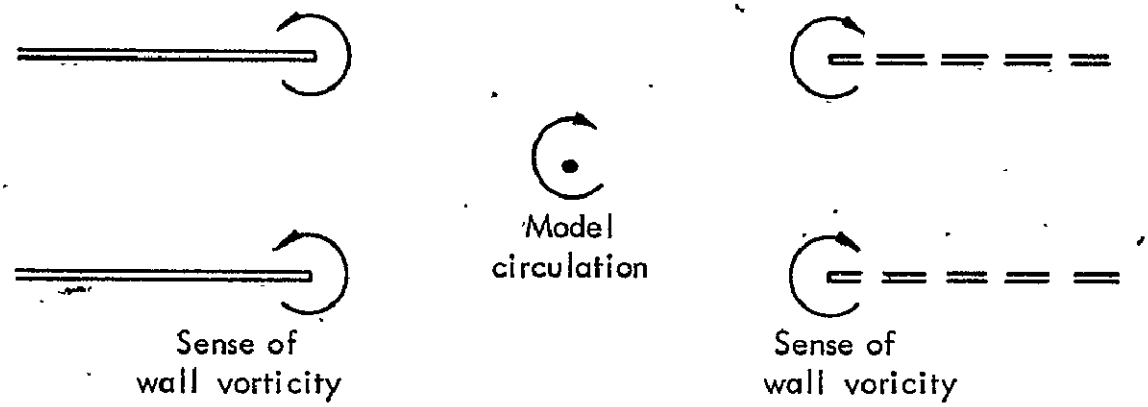

b) Solid/open jet terminations.

FIG. 4.5, SENSE OF END SECTION INTERFERENCE.

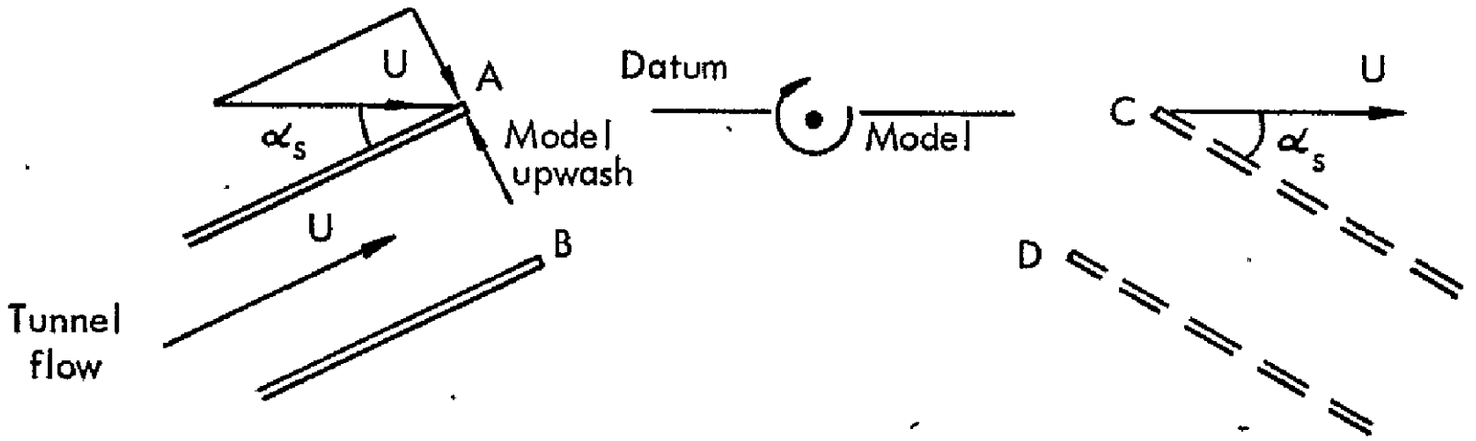

FIG. 4.6. FLOW TURNING AND EQUIVALENT FREE STREAM.

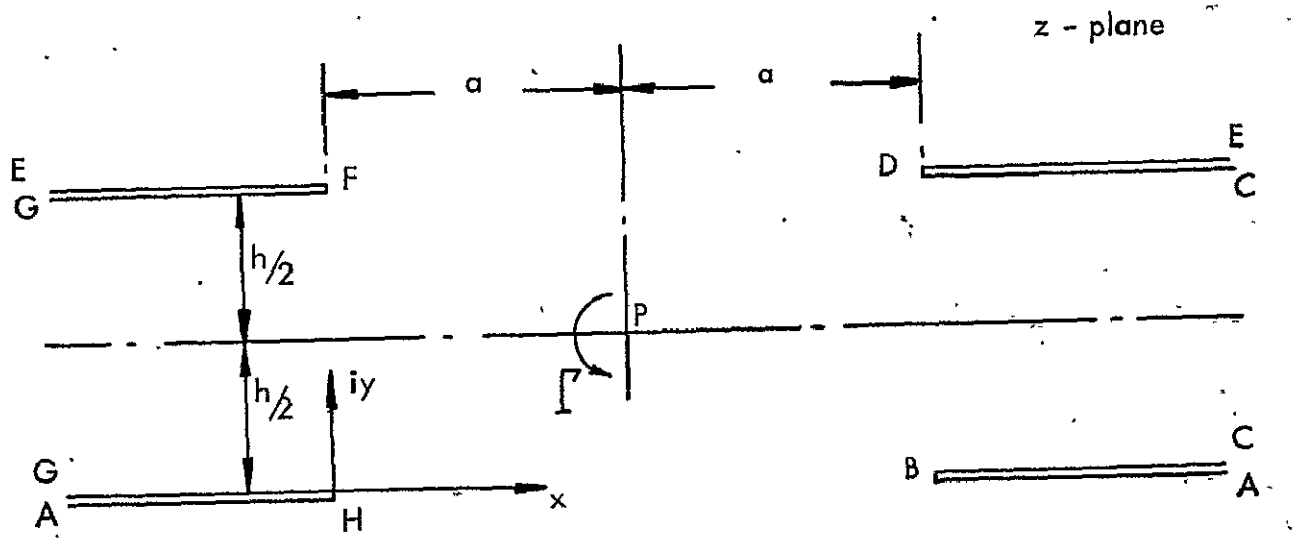

(a) Complex z - plane

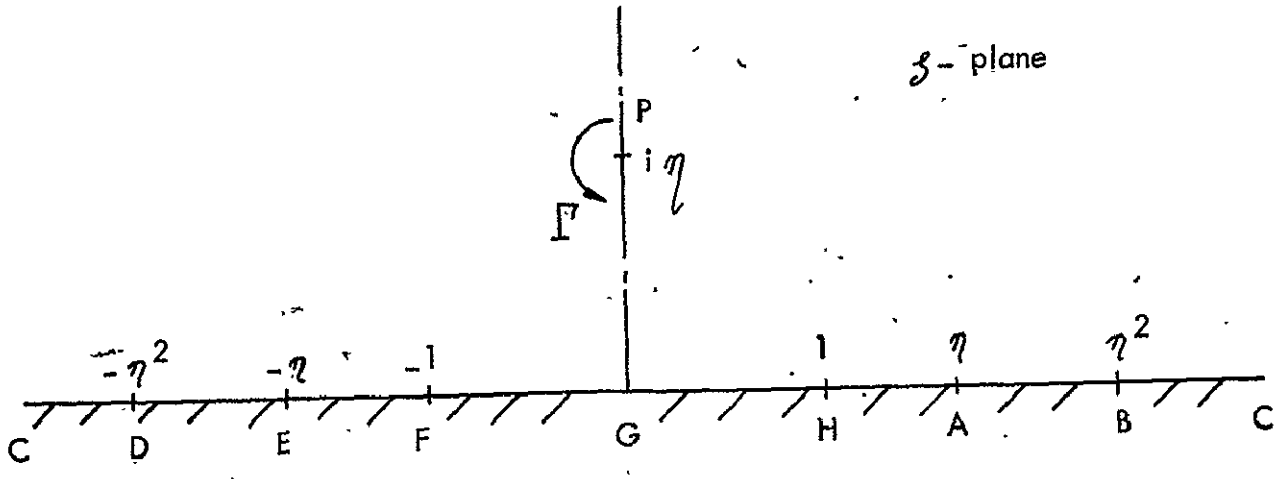

(b) Transformed ζ - plane,

FIG. 4.7. PHYSICAL AND TRANSFORMED PLANES.

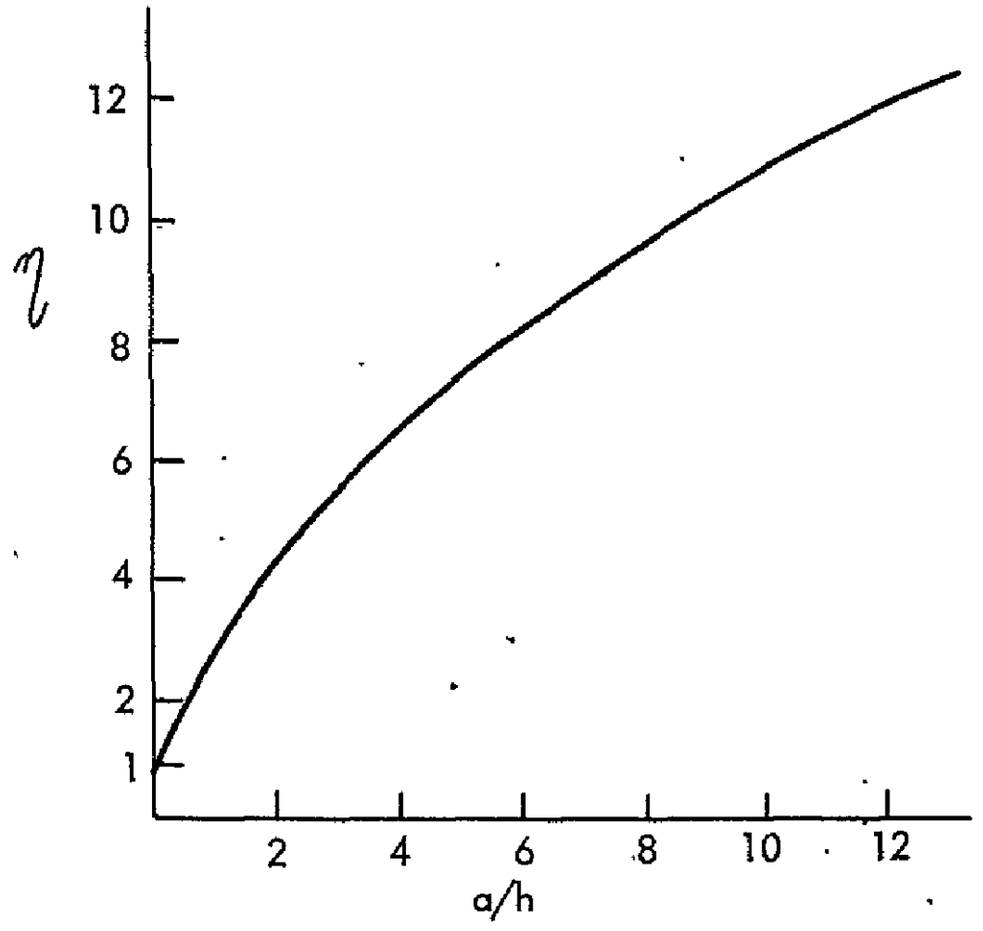

FIG. 4.8. VARIATION OF PARAMETER η WITH TUNNEL SEMI-LENGTH/ HEIGHT RATIO.

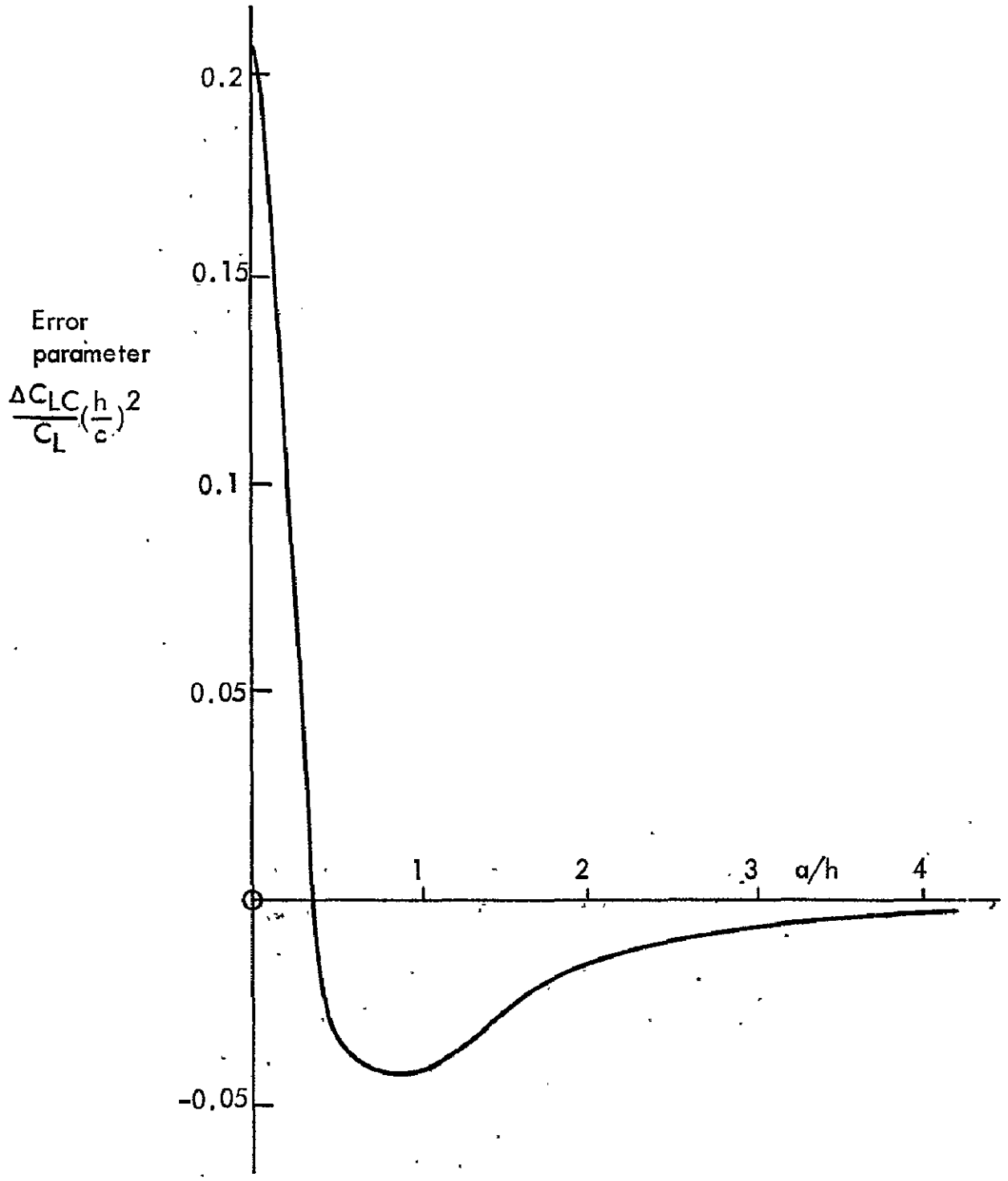

FIG. 4.9. VARIATION OF THE LIFT ERROR PARAMETER WITH TUNNEL SEMI-LENGTH/HEIGHT RATIO.

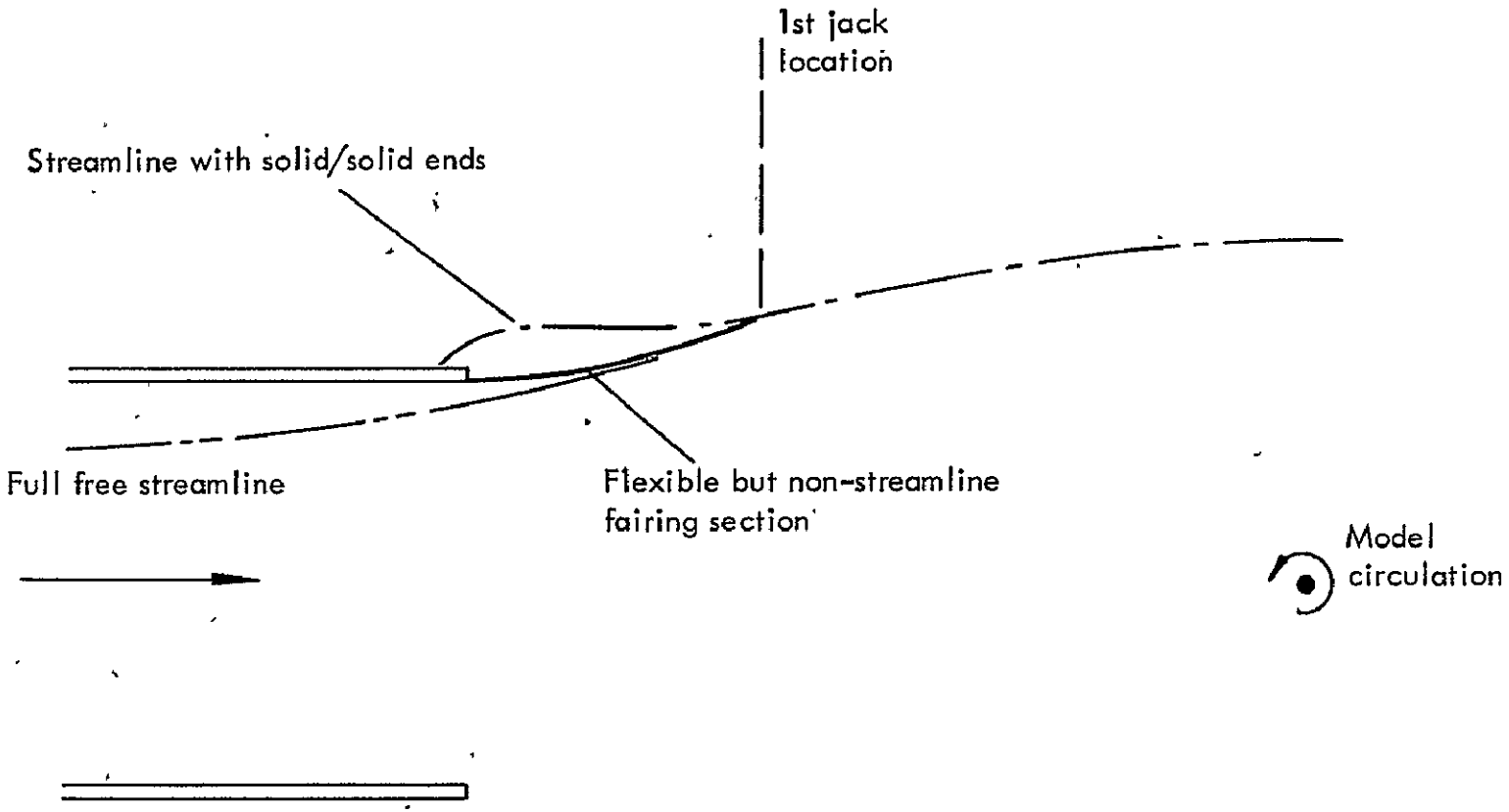

FIG. 4.10. FLOW DETAILS AT FLEXIBLE SECTION ENDS.

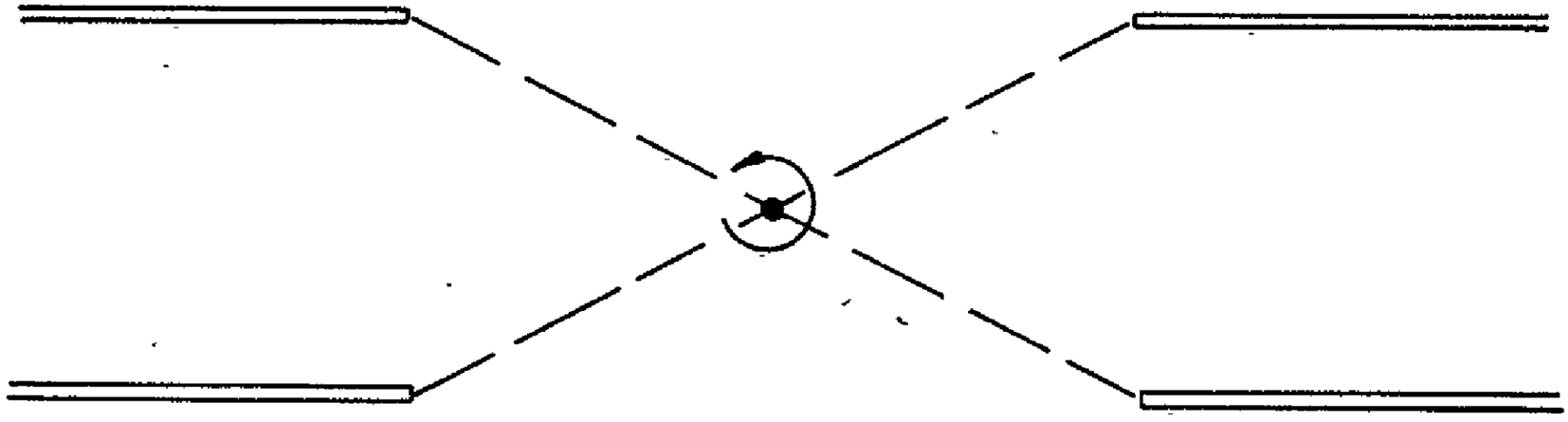

FIG. 4.11. MODEL LOCATION FOR ZERO UPWASH CORRECTION.

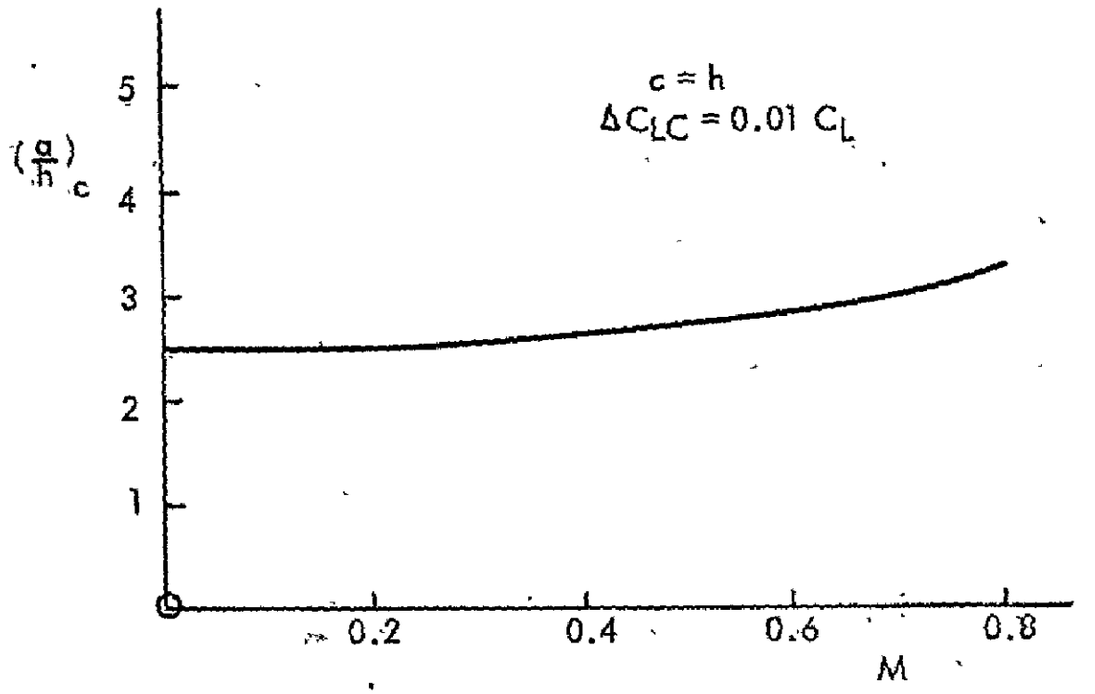

FIG. 4.12. VARIATION OF REQUIRED TUNNEL SEMI-LENGTH/HEIGHT RATIO WITH MACH NUMBER.

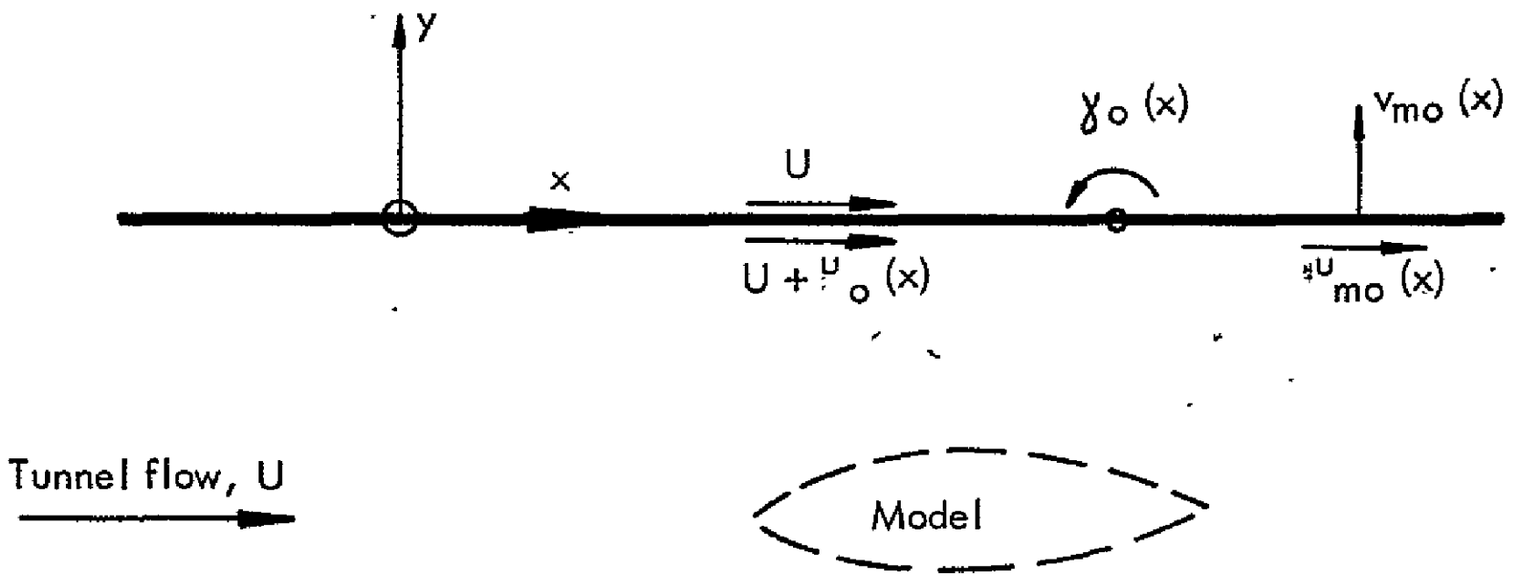

FIG. 5.1. INITIAL WALL ARRANGEMENT

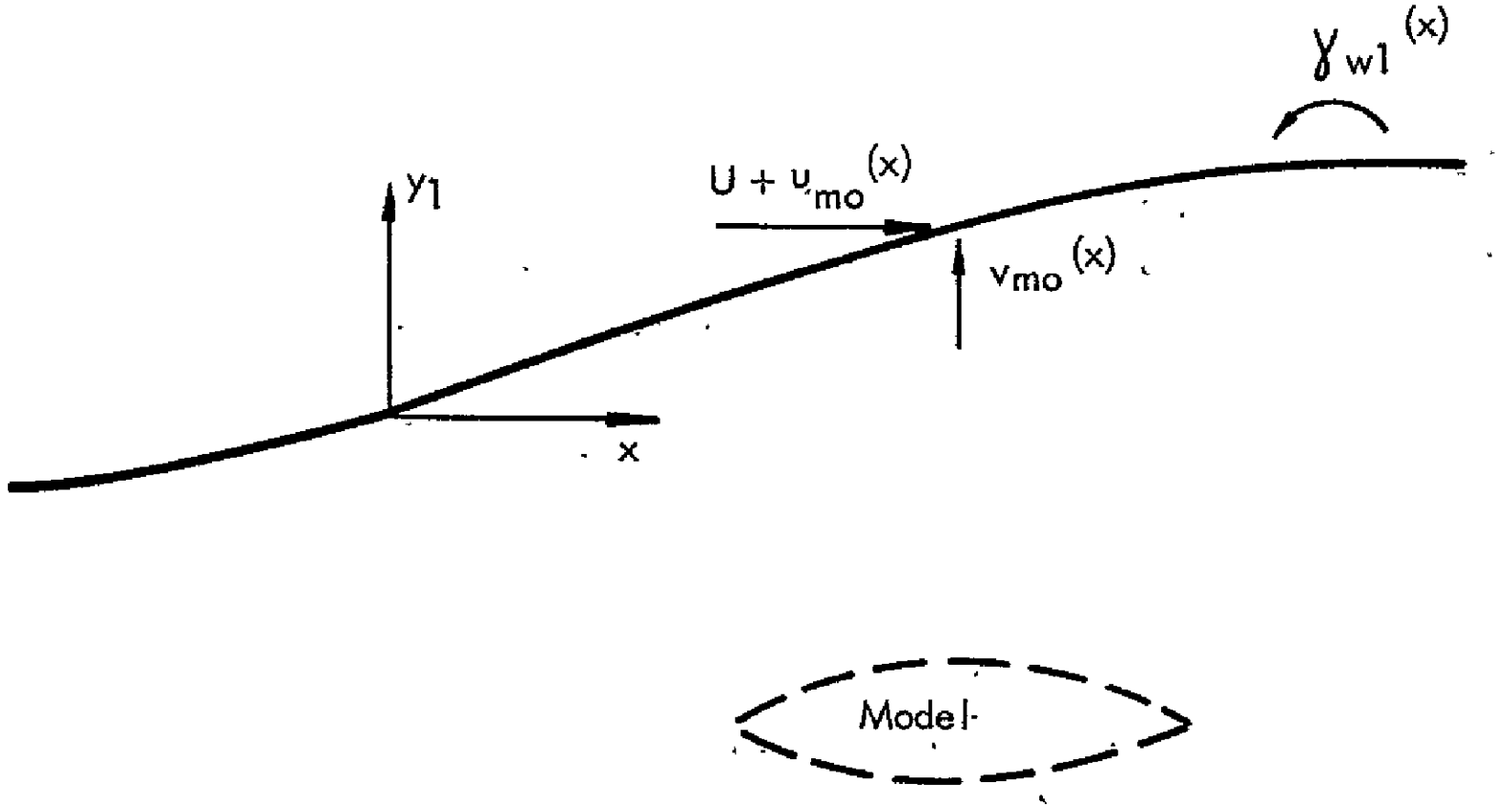

FIG. 5.2. MODIFIED WALL POSITION.